AGU PUBLICATIONS

JGR

Journal of Geophysical Research: Atmospheres

RESEARCH ARTICLE

10.1002/2014JD022453

Key Points:
- New enhanced MODIS Collection 6 aerosol data available
- This study compares and validates the two over-land algorithms used
- Usage recommendations are provided

Correspondence to:
A. M. Sayer,
andrew.sayer@nasa.gov

Citation:
Sayer, A. M., L. A. Munchak, N. C. Hsu, R. C. Levy, C. Bettenhausen, and M.-J. Jeong (2014), MODIS Collection 6 aerosol products: Comparison between Aqua's e-Deep Blue, Dark Target, and "merged" data sets, and usage recommendations, *J. Geophys. Res. Atmos.*, *119*, 13,965–13,989, doi:10.1002/2014JD022453.

Received 15 AUG 2014
Accepted 7 NOV 2014
Accepted article online 17 NOV 2014
Published online 20 DEC 2014

MODIS Collection 6 aerosol products: Comparison between Aqua's e-Deep Blue, Dark Target, and "merged" data sets, and usage recommendations

A. M. Sayer[1,2], L. A. Munchak[1,3], N. C. Hsu[1], R. C. Levy[1], C. Bettenhausen[1,3], and M.-J. Jeong[4]

[1]NASA Goddard Space Flight Center, Greenbelt, Maryland, USA, [2]Goddard Earth Sciences Technology and Research, Universities Space Research Association, Greenbelt, Maryland, USA, [3]Science Systems and Applications, Inc., Lanham, Maryland, USA, [4]Department of Atmospheric and Environmental Sciences, Gangneung-Wonju National University, Gangneung City, Gangwong Province, Korea

Abstract The Moderate Resolution Imaging Spectroradiometer (MODIS) Atmospheres data product suite includes three algorithms applied to retrieve midvisible aerosol optical depth (AOD): the Enhanced Deep Blue (DB) and Dark Target (DT) algorithms over land, and a DT over-water algorithm. All three have been refined in the recent "Collection 6" (C6) MODIS reprocessing. In particular, DB has been expanded to cover vegetated land surfaces as well as brighter desert/urban areas. Additionally, a new "merged" data set which draws from all three algorithms is included in the C6 products. This study is intended to act as a point of reference for new and experienced MODIS data users with which to understand the global and regional characteristics of the C6 DB, DT, and merged data sets, based on MODIS Aqua data. This includes validation against Aerosol Robotic Network (AERONET) observations at 111 sites, focused toward regional and categorical (surface/aerosol type) analysis. Neither algorithm consistently outperforms the other, although in many cases the retrieved AOD and the level of its agreement with AERONET are very similar. In many regions the DB, DT, and merged data sets are all suitable for quantitative applications, bearing in mind that they cannot be considered independent, while in other cases one algorithm does consistently outperform the other. Usage recommendations and caveats are thus somewhat complicated and regionally dependent.

1. Introduction

Knowledge of the global atmospheric aerosol burden is of importance for a number of research areas, such as understanding the radiation budget of the Earth system [e.g., *Schulz et al.*, 2006], air quality and human health [*Pope et al.*, 2002], ecosystem fertilisation [*Tian and An*, 2013], aviation safety [*Guffanti et al.*, 2010], visibility forecasting [*Zhang and Reid*, 2006], and solar energy yields [*Murphy*, 2009]. Due to the high spatiotemporal variability of aerosol loading, satellite observations can make an important contribution to research in these areas. However, past and present satellite instruments have insufficient measurement capabilities to determine the relevant aerosol parameters of interest to within the uncertainties desired for some of these applications [e.g., *Hasekamp and Landgraf*, 2007; *Kokhanovsky et al.*, 2010; *Kahn*, 2012]. For radiative calculations, the key aerosol parameters are the spectral aerosol optical depth (AOD), directional dependence of scattering (i.e., phase matrix), spectral single scattering albedo (SSA), and vertical profile. In contrast, applications such as air quality focus more on the total mass of particles near the surface (often particulate matter smaller than 2.5 or 10 μm diameter, termed $PM_{2.5}$/PM_{10}, respectively) than on optical metrics.

The diversity in Earth-observing satellite instruments has led to the development of many different aerosol remote sensing algorithms; discussion of different sensors/algorithms and their strengths and limitations is provided by, e.g., *Mishchenko et al.* [2007], *Kokhanovsky and de Leeuw* [2009], *Li et al.* [2009], *Mishchenko et al.* [2010], *Hyer et al.* [2011], *Kahn et al.* [2011], *Kahn* [2012], and references therein. The most commonly retrieved parameters are the midvisible AOD and the Ångström exponent α, which describes the spectral dependence of AOD over a given wavelength range. One sensor (among many) is the Moderate Resolution Imaging Spectroradiometer (MODIS), for which three AOD retrieval algorithms are processed routinely as part of NASA's MODIS Atmospheres product suite. Over land, these are known as Dark Target (DT) and Deep Blue (DB); DT [*Kaufman et al.*, 1997; *Levy et al.*, 2013] was developed to work over dense, dark vegetation while DB was originally [*Hsu et al.*, 2004] developed to fill in the gaps in DT by providing coverage over

brighter surfaces (such as deserts). The third algorithm [*Tanré et al.*, 1997; *Levy et al.*, 2013] is applied over water surfaces and is also a "Dark Target" approach in that it relies on midvisible and longer wavelengths at which the water surface is dark, although the DT land and ocean algorithms are algorithmically independent from each other. A combined DT land/ocean scientific data set (SDS) has also been (and still is) provided in the MODIS Level 2 (orbit-level) data products. Because of the over-land focus of this study, the term DT is used hereafter to refer to only the over-land algorithm.

Recently, the MODIS Collection 6 (C6) data product suite has been released. This multidisciplinary effort contains refinements to all three aerosol algorithms [*Hsu et al.*, 2013; *Levy et al.*, 2013; *Sayer et al.*, 2013], as well as considerable work by the MODIS Characterization Support Team (MCST) and Ocean Biology Processing Group (OBPG) to maintain or improve the high radiometric quality of MODIS top-of-atmosphere (TOA) radiance measurements through the time series [e.g., *Meister and Franz*, 2011; *Meister et al.*, 2012; *Wu et al.*, 2013]. Aerosol algorithmic refinements have been driven in part by studies which identified various shortcomings and contextual biases of the previous versions [e.g., *Zhang and Reid*, 2006; *Levy et al.*, 2010; *Bréon et al.*, 2011; *Hyer et al.*, 2011; *Shi et al.*, 2011, 2013; *Huang et al.*, 2013]. The previous reprocessings were known as Collection 5 (C5) and Collection 5.1 (C5.1); the same aerosol algorithm versions were included in the C5 and C5.1 processings, which are hereafter referred to as C5 for simplicity.

In C6 the capabilities of the DB algorithm have been expanded to cover all cloud-free snow-free land surfaces, and the new algorithm version is also referred to as "enhanced Deep Blue" to distinguish it from the C5 algorithm. As a result of this expanded coverage, over much of the world both DB and DT data are available. An additional, "merged," SDS is now also provided in the MODIS aerosol products, combining the DB with DT land/ocean data. This study provides a first comparison and evaluation of the C6 DB, DT, and merged data sets against each other and Aerosol Robotic Network (AERONET) [*Holben et al.*, 1998] ground-truth data, with the intent of identifying their strengths and weaknesses and helping users to identify the most appropriate of the data set(s) to use for their particular application. The focus of this effort is on comparison and evaluation of the over-land data sets; *Sayer et al.* [2012a] and *Levy et al.* [2013] provide discussion and some evaluation of the C6 over-ocean algorithm and comparisons to C5. Section 2 provides more detail on the DB and DT algorithms and merging process, and section 3 a detailed comparison of the data sets with each other. Section 4 presents the evaluation methodology to compare the three against AERONET, and section 5 provides discussion of results and some usage recommendations from global and regional perspectives.

2. MODIS Data Set Descriptions

Two MODIS sensors are in operation, launched to Sun-synchronous polar orbits on the Terra platform (10:30 A.M. local solar Equatorial crossing time) in late 1999 and on the Aqua platform (1:30 P.M. local solar Equatorial crossing time) in 2002. MODIS is a passive imaging radiometer and measures reflected solar and emitted thermal radiation in 36 bands, across a 2330 km swath (providing near-daily global coverage at the Equator and overlap between orbits at higher latitudes). Spatial resolutions are between 250 m and 1 km at nadir (dependent on band) but become progressively larger at the edge of the swath, by a factor of up to ~2 along-track and ~5 across-track. The DB and DT data sets are both provided at a nominal (nadir) spatial resolution of 10×10 km. Spatiotemporally aggregated "Level 3" products at 1° × 1° horizontal and daily, 8 day, and monthly temporal resolution are also available.

These data sets are distributed freely in hdf4 format from http://ladsweb.nascom.nasa.gov/ as the M*x*D04_L2, M*x*DATML2, and M*x*D08 data products (*x* is O for MODIS Terra and Y for MODIS Aqua). The DT land and ocean algorithms are also used to create a separate data product at 3×3 km [*Remer et al.*, 2013], although this has no DB equivalent, and is not used in the merged product or propagated into Level 3 products, so is not further discussed here. Additional documentation and browse imagery can be found at http://modis-atmos.gsfc.nasa.gov/.

Throughout this study, the retrieval data product evaluated is the AOD at 550 nm, which is the primary data product from the DB and DT algorithms, denoted τ_{DB} and τ_{DT}, respectively, or as τ_{M} (M for "MODIS") when in a generic context not specific to one algorithm. Unless specified otherwise, references to AOD indicate AOD at 550 nm, and only retrievals passing recommended quality assurance (QA) checks [*Hsu et al.*, 2013; *Levy et al.*, 2013; *Sayer et al.*, 2013] are used (for DB, corresponding to retrievals flagged QA=2 or QA=3; for DT, retrievals flagged QA=3). This QA filtering is to match the analysis to the intended way in which most users will approach the data sets. Table 1 provides the names for the relevant SDS within the MODIS Level

Table 1. Relevant Level 2 SDS Names and Contents for QA-Filtered MODIS AOD at 550 nm

SDS Name	Contents
AOD_550_Dark_Target_Deep_Blue_Combined	The "merged SDS:" DB, DT, or their average over land; ocean algorithm over ocean.
AOD_550_Dark_Target_Deep_Blue_Combined_Algorithm_Flag	Indicates the algorithm populating each pixel of the merged SDS.
Optical_Depth_Land_And_Ocean	Union of DT land and ocean data.
Deep_Blue_Aerosol_Optical_Depth_550_Land_Best_Estimate	DB over land, no data over ocean.

2 aerosol products. Only C6 data from MODIS Aqua are used in this analysis as Terra C6 data are not yet available, although they are expected to be quantitatively similar.

2.1. Dark Target

The C6 implementation of the DT algorithm [*Levy et al.*, 2013] includes refinements and code bugfixes but is based on the same principles as the C5 version, described by *Levy et al.* [2007], which builds on the heritage of the initial implementation [*Kaufman et al.*, 1997]. First, measured TOA reflectances within each 10×10 km retrieval box are screened to remove unsuitable (e.g., cloud, desert, snow/ice, and inland water) pixels; an additional fraction of the darkest and brightest pixels is discarded, and the remaining pixel-level reflectances averaged. Then, the shortwave IR (swIR) TOA reflectance is related to surface reflectance at visible wavelengths (470 nm and 650 nm) via an assumed spectral/directional relationship, which are then used to determine the total AOD from a weighted combination of fine-mode dominated and coarse-mode (dust) dominated aerosol models by matching the averaged TOA reflectance at these wavelengths. The fine-dominated model used for a given retrieval is determined by location on the globe and season. The DT algorithm is not applied over scenes identified by internal tests as bright land surfaces (e.g., deserts, snow), as the swIR-to-visible surface reflectance relationship does not hold for these surface types.

The estimated 1 standard deviation absolute uncertainty confidence envelope for the DT algorithm (for QA=3 data), often referred to as "expected error" (EE_{DT}), has been determined on global average [*Levy et al.*, 2010, 2013] to be $\pm(0.05+0.15\tau_A)$, where τ_A is the AERONET-observed AOD (i.e., a diagnostic uncertainty estimate). This AOD dependence of uncertainty arises because in low-AOD conditions the total uncertainty is dominated by surface reflectance assumptions while as AOD increases assumptions related to aerosol properties (most notably SSA and spectral slope of AOD), which scale with AOD, become increasingly dominant.

2.2. Deep Blue

MODIS C6 includes a heavily revamped and extended version of the original DB algorithm and is described by *Hsu et al.* [2013]. Unlike DT, DB performs retrievals on cloud-free and snow-free pixels at nominal 1×1 km spatial resolution and then aggregates afterward to the 10×10 km retrieval box. Retrievals are performed over bright desert surfaces, in addition to vegetated surfaces. Surface reflectance is prescribed by one of several methods, dependent on location, season, and land cover type: from a database as a function of location, season, scattering angle, and normalized difference vegetation index (NDVI); from an empirically derived bidirectional reflectance distribution function (BRDF) for a given region and season; or from a spectral/directional relationship (similar to the DT method) for a given land surface classification type. The algorithm retrieves AOD individually at each of 470 and/or 412/650 nm (dependent on surface type), for an assumed aerosol optical model (as a function of location and season), and then determines the combination of AOD (at 550 nm) and α which is most consistent with the retrieved spectral AOD. In low-AOD conditions, α is set to a fill value (1 over deserts, 1.5 elsewhere), and in high-AOD

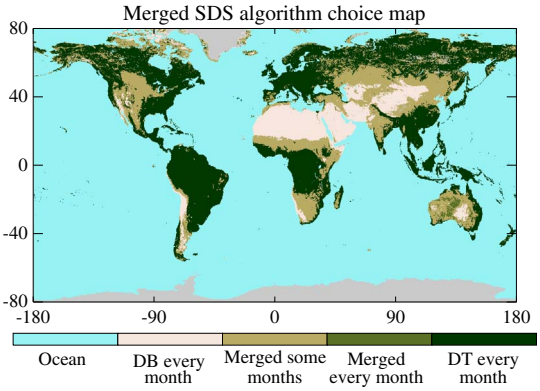

Figure 1. Regional algorithm choices for the "merged" SDS included in MODIS C6 aerosol data. Regions in grey lack valid NDVI (as well as valid AOD retrievals).

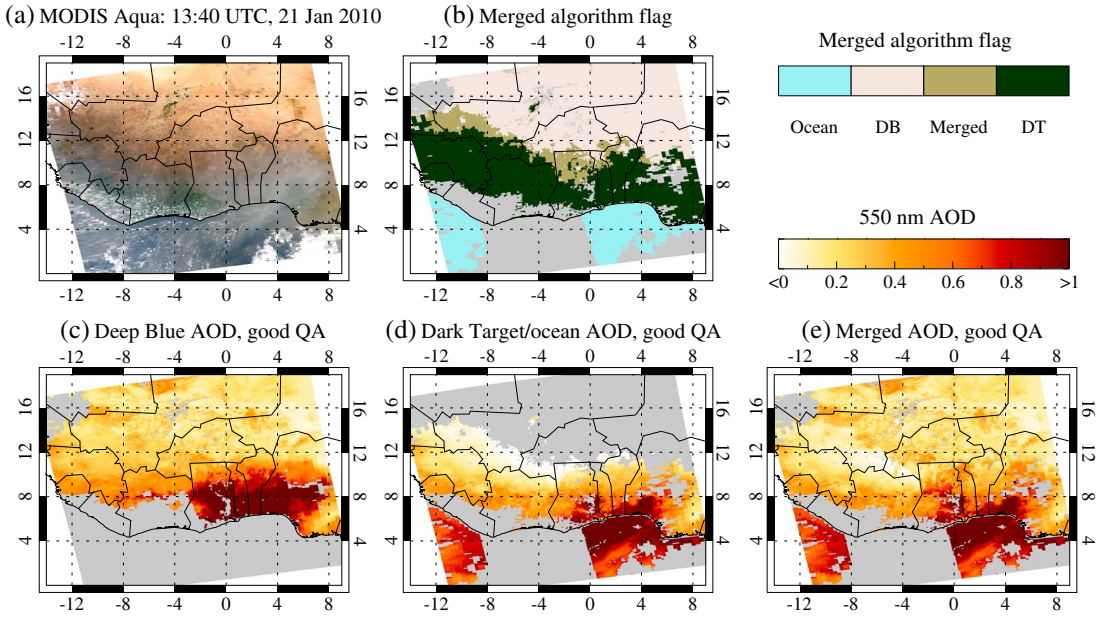

Figure 2. Example of the merging process for a MODIS Aqua granule over the Sahel. (a) A true-color image and (b) the algorithms selected for each individual retrieval (cf. Figure 1). (c–e) DB, DT land/ocean, and merged AOD, respectively. Regions in grey lack valid AOD retrievals.

conditions with a sufficiently dark surface reflectance, the spectral SSA is also retrieved by using a maximum likelihood method to pick between one of a set of aerosol optical models.

Sayer et al. [2013] validated DB data against AERONET to determine empirical 1 standard deviation absolute uncertainty confidence envelopes, which depend on the AOD, QA flag, and viewing geometry. These uncertainty estimates for DB are provided within the data products for each retrieval. For QA=3 data (highest quality), this expected error (EE_{DB}) was found to be $\pm([0.086+0.56\tau_{DB}]/[1/\mu_0+1/\mu])$, where $1/\mu_0+1/\mu$ is the sum of the reciprocal cosines of solar and view zenith angles for a given retrieval. Unlike the DT uncertainty estimate, this is a prognostic uncertainty (i.e., defined relative to DB-retrieved AOD rather than to AERONET AOD). As a typical value, $1/\mu_0+1/\mu \approx 2.8$, such that $EE_{DB} \approx \pm(0.03+0.20\tau_{DB})$, comparable to the DT uncertainty for typical aerosol loadings (AOD $\sim 0.1-0.5$).

2.3. Merging Procedure

The inclusion of a merged SDS within the C6 aerosol products was motivated by a desire to provide a more gap-filled data set than is available from the individual algorithms alone. Hereafter, the discussion focusses on retrievals rather than sensor pixels, and so the term "pixel" is used to refer to the (nominal) 10×10 km spatial resolution retrievals rather than the raw (higher-resolution) sensor measurements.

The logic behind the merge as implemented within the C6 reprocessing was that there is a longer heritage of user familiarity with DT data over densely vegetated regions, while DB is the only data set providing coverage over arid surfaces. Three classifications were determined by aggregating MODIS-derived climatologies of NDVI (the MYD13C2 data set) [*Huete et al.*, 2011] to 0.25° spatial resolution for each month of the year. Over land, where NDVI≤0.2 in a given month, DB data are used to populate the merged SDS, and where NDVI ≥0.3, DT data are used. For intermediate NDVI (often transition zones between arid and vegetated land), the algorithm whose retrieval returns the higher QA flag is used, or if both return QA=3, the mean value is used. This empirical approach was designed to be simple and transparent to the end-user, and there is scope to revisit it in the future; a SDS is provided within the Level 2 data products so that users may identify which of these three NDVI regimes each individual retrieval falls into (see Table 1). All over-ocean scenes in the merged SDS are populated using the ocean algorithm. The merged SDS is only populated for those pixels where the appropriate algorithm's retrieval is assigned a sufficiently high QA flag to be deemed usable by the algorithm team (QA≥2 for DB, QA=3 for DT, QA≥1 for ocean). Note that QA tests and quality definitions are different for the three AOD retrieval algorithms (the 0–3 scale used is shared convention rather than implying commonality of definitions) and that only over-land pixels are analysed in this study.

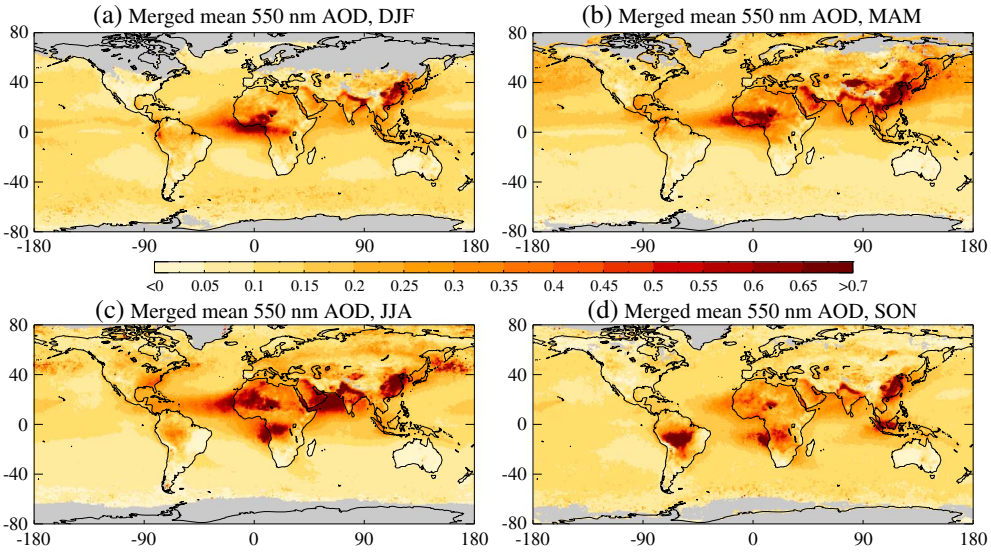

Figure 3. Seasonal mean AOD from the "merged" SDS for 2006–2008, at 1° × 1° horizontal resolution, for (a) December-January-February (DJF), (b) March-April-May (MAM), (c) June-July-August (JJA), and (d) September-October-November (SON). Grid cells with fewer than 3 days containing valid data in a season are shaded in grey.

Figure 1 shows an annual composite of these classifications. The category "merged some months" indicates grid cells where in some months the NDVI falls into this transitionary range (0.2–0.3) and in others DB/DT are assigned, while "merged all months" indicates regions where the climatological NDVI always falls within this range. Thus, DB is chosen largely over deserts, DT over largely perpetually vegetated regions, and the potential merging zone borders these two, moving dependent on the seasonal growth and senescence of vegetation.

Figure 2 provides an example for a MODIS granule over the Sahel; the resultant merged AOD field is more spatially complete than either the DB or DT AOD fields, although as is an inherent danger in any data set created from multiple algorithms, the merging may also introduce discontinuities. For this specific example, there are discontinuities between the DT land and ocean algorithms under the heavy aerosol visible around 0–8°N, 0–8°E, and in the "merged" data set along the line where its source switches between DB and DT (from 16°N, 12°W to 4°N, 4°W). On a global basis, Figure 3 shows seasonal mean AOD calculated from the merged SDS. Residual gaps in coverage are associated with persistent cloud/snow cover and polar night; otherwise, the regional and seasonal patterns are similar to results obtained from other satellite sensors and model simulations [e.g., *Kinne et al.*, 2006].

3. Comparison Between MODIS Data Sets

Previous validation and comparison exercises have identified regime-specific biases in the over-land C5/C6 MODIS aerosol data sets, from both globally [*Levy et al.*, 2010, 2013; *Bréon et al.*, 2011; *Hyer et al.*, 2011; *Shi et al.*, 2011, 2013; *Sayer et al.*, 2013] and regionally focussed [*Li et al.*, 2007; *Drury et al.*, 2008; *Li et al.*, 2009; *Jethva et al.*, 2010; *Wang et al.*, 2010; *Bennouna et al.*, 2011; *Banks et al.*, 2013; *Eck et al.*, 2013] studies. Thus, this section examines regionally and globally aggregated C6 data to note their similarities and differences.

3.1. Mapped Collocated Pixel-Level Data

This analysis uses only those pixels where both DB and DT algorithms provided a retrieval passing QA checks during 2006–2008. As a result of the requirement for pixel-level matching between the algorithms, no data remain over water or bright desert surfaces. Figure 4 shows the seasonal mean (computed as mean of daily means) AOD from the DB and DT data sets, and their difference ($\tau_{DB} - \tau_{DT}$). Seasonal median AOD and difference maps (not shown) have very similar spatial patterns over much of the world to these seasonal means. This happens as the bulk of the data in many regions/seasons are for low-AOD conditions; these persistent offsets between the two data sets are likely due in large part to surface reflectance assumptions. In a few areas (e.g., smoke from wildfires in north-eastern Russia in JJA, smoke in South America during SON),

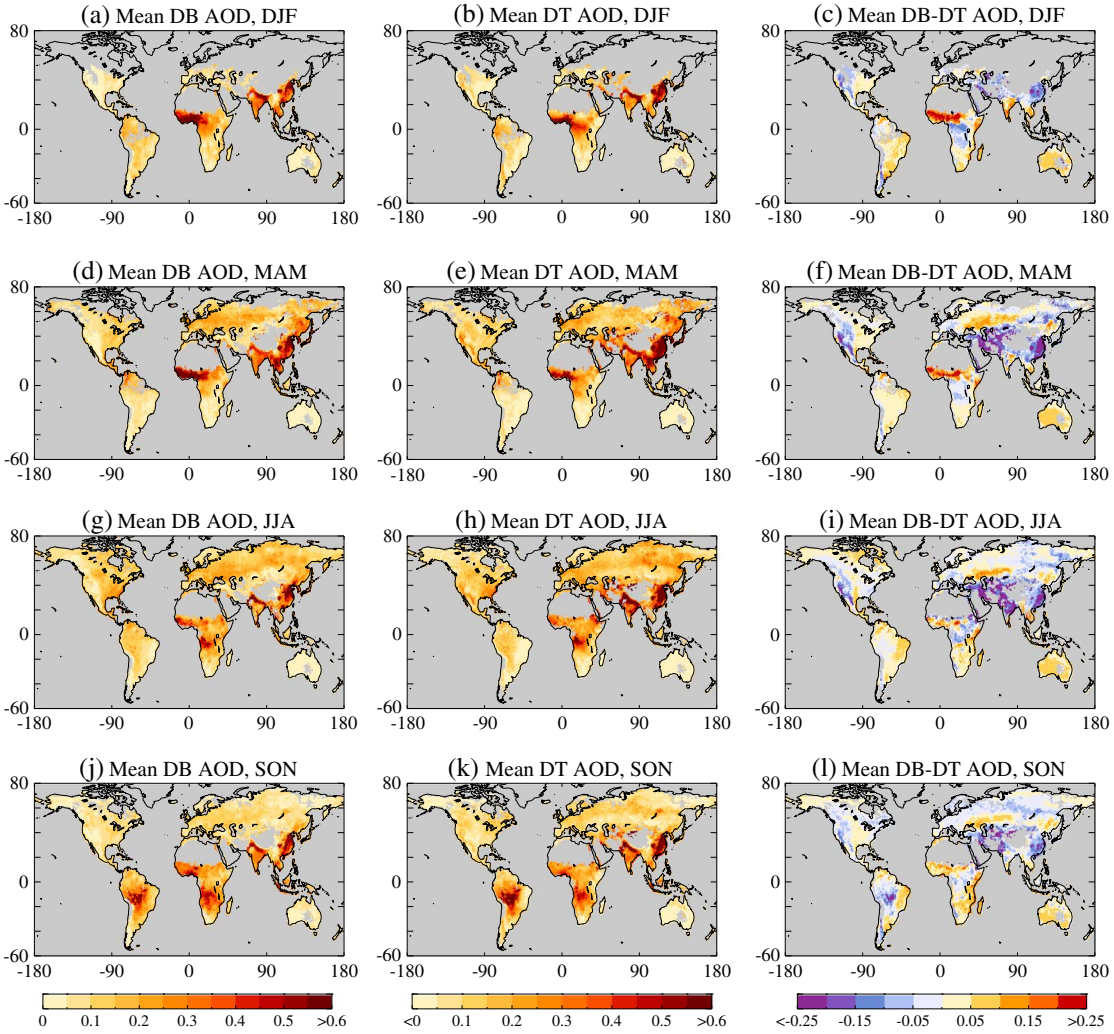

Figure 4. Seasonal mean AOD for 2006–2008, at 1° × 1° horizontal resolution, for (left) Deep Blue and (middle) Dark Target. (right) The difference (DB−DT) in the mean AOD. Grid cells with fewer than 3 days containing valid data in a season are shaded in grey.

median AODs and $\tau_{DB} - \tau_{DT}$ are smaller than the mean values. These are cases where sporadic high-AOD events (and corresponding larger retrieval uncertainties) are contributing more to Figure 4.

With a few notable exceptions, the mean (and median) differences between DB and DT data are less than 0.05 over large parts of the world. In locations where DT frequently retrieves negative AOD (caatinga/cerrado surfaces of the Sertão in Brazil, and much of Australia), the difference is typically 0.05–0.1 as DB retrieves small positive AOD. The mean $\tau_{DB} - \tau_{DT}$ is positive in the Sahel and negative in south-eastern Asia; these are high-AOD regions which contain dust (albeit from different sources and with potentially different optical properties), smoke, and industrial aerosols, such that assumptions related to aerosol optical properties are likely to contribute to differences between AOD retrieved by the two algorithms frequently.

Interestingly, for India $\tau_{DB} - \tau_{DT}$ is negative in JJA (approximately −0.15) and small or positive in other seasons, such that DT reports a larger seasonal variability of AOD. Observational [*Gautam et al.*, 2010] and model [*Henriksson et al.*, 2011] studies concerning the seasonal contribution of different aerosol types to the total AOD in India show that mineral dust makes a large contribution to total AOD during the pre-monsoon season (April–June) while at other times of the year anthropogenic fine-mode-dominated aerosols are optically more dominant. As this is a densely populated region, there is considerable interest in understanding the aerosol loading and its changes through time here from radiative, meteorological, and health perspectives [*Garg et al.*, 2006; *Ramanathan et al.*, 2007; *van Donkelaar et al.*, 2010; *Dey and Di Girolamo*, 2011; *Hsu et al.*, 2012], and, given the utility of satellite data for this task, it is suggested that future work should aim to

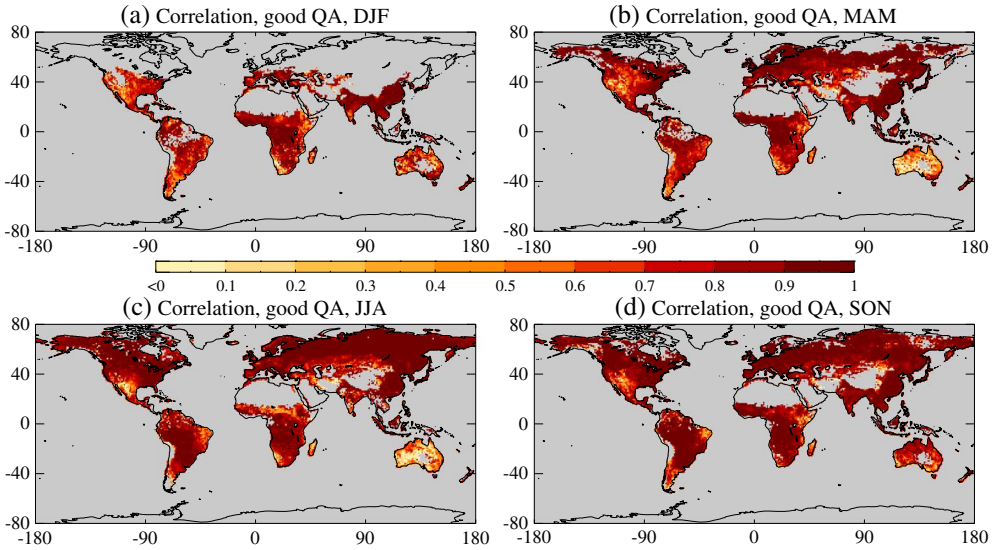

Figure 5. Correlation between daily Deep Blue and Dark Target AOD on a seasonal basis, for (a) DJF, (b) MAM, (c) JJA, and (d) SON. Grid cells with fewer than 3 days containing valid data in a season are shaded in grey.

understand these discrepancies between the DB and DT data sets such that they can be resolved in future versions of the algorithm. Although an in-depth regional analysis is out of the scope of this study, validation against AERONET in section 4 does provide an assessment (discussed later) of the likely reliability of both algorithms globally and regionally.

The correlation between daily mean AOD retrieved by both algorithms within a given season is high (Figure 5), typically above 0.9, aside from persistently low-AOD regions where the magnitude of day-to-day variability in AOD is small compared to retrieval uncertainty. This indicates that both algorithms track the same changes in AOD. The results in this section are quantitatively similar (not shown) if data are matched on a daily 1° basis, rather than a 10 km pixel-level basis, suggesting that the primary differences between DB and DT data on these spatial/temporal scales are related to algorithmic assumptions rather than pixel selection.

Considering the high correlation between DB and DT retrievals shown in Figure 5, it is worth examining the level of agreement between individual retrievals and to understand how frequently retrievals are in agreement with each other relative to their stated uncertainties (EE_{DB} and EE_{DT}; section 2). Although DT provides a diagnostic rather than prognostic error estimate, if it is assumed that on average DT provides an unbiased estimate of the true AOD for a given regime (i.e., for a given atmospheric/surface regime, over a large ensemble of observations, $\bar{\tau}_{DT} = \bar{\tau}_{A}$), it would be reasonable to treat EE_{DT} as prognostic and create uncertainty estimates on a per-pixel basis. Note that this assumption does not necessarily hold true for high-AOD conditions, but biases in low-AOD conditions are small (see section 5). Then, if EE_{DB} and EE_{DT} represent unbiased Gaussian 1 standard deviation uncertainty confidence intervals on retrieved AOD, and if the errors in DB and DT retrievals are independent of each other, then 1 standard deviation (i.e., 68%) of individual retrieval differences $\tau_{DB} - \tau_{DT}$ should fall within the quadrature sum of these uncertainties, i.e., $\pm\sqrt{(EE_{DB}^2 + EE_{DT}^2)}$.

Figure 6 shows, on a seasonal basis, the fraction of retrievals where the absolute difference between retrievals $|\tau_{DB} - \tau_{DT}|$ is smaller than $\sqrt{(EE_{DB}^2 + EE_{DT}^2)}$. It is immediately apparent that the majority of the land surface is shaded in red tones, indicating that greater than 68% of matched retrievals are more similar to each other than this combined uncertainty estimate would suggest. Indeed, in many areas this figure is over 90%. This indicates regions where the uncertainties in the the two algorithms are therefore not independent of each other and/or are smaller than the stated expressions for EE_{DB} and EE_{DT}. It is important to emphasise that this agreement between the two data sets in retrieved AOD does not imply that both are "true"; it may also show areas where the two algorithms make similar assumptions, which may or may not be appropriate.

In contrast, in semiarid and/or elevated regions (e.g., the Sahel, south-western Asia, southern tip of Africa, and south-western North America), regions where DT retrieves negative AOD (the Sertão region of Brazil;

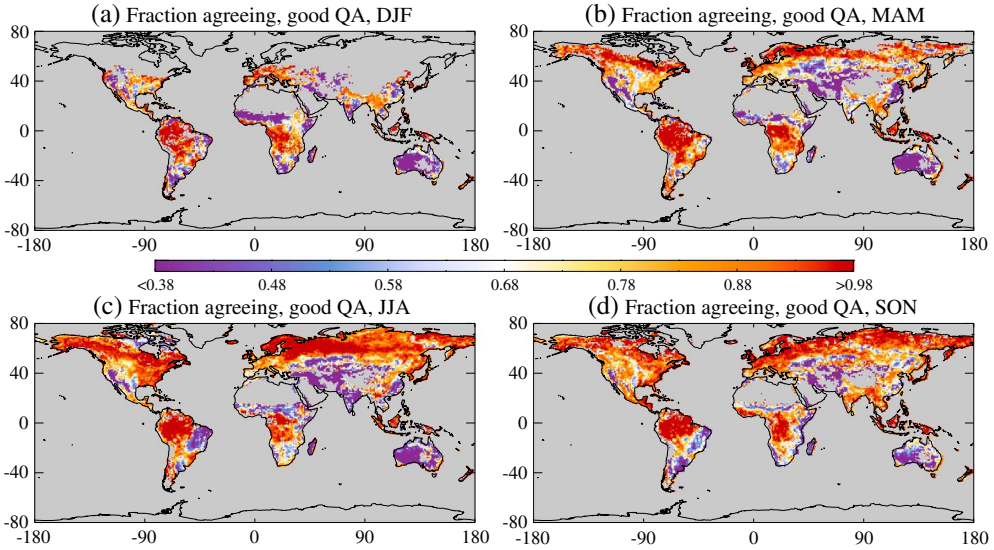

Figure 6. Seasonal fraction of matched retrievals whose absolute difference is smaller then the quadrature sum of their expected uncertainties, for (a) DJF, (b) MAM, (c) JJA, and (d) SON. Grid cells with fewer than 3 days containing valid data in a season are shaded in grey.

Australia), and high-AOD regions (e.g., India and south-eastern Asia), fewer than 40% of matched retrievals are in agreement, indicating areas where algorithmic uncertainties are anticorrelated and/or larger than stated. Accordingly, these are the regions that show some of the largest differences in seasonal mean AOD between the two data sets in Figure 4.

This comparison shows that the DB and DT data sets should not be considered statistically independent of one another and that there are regions where they are persistently more or less frequently in agreement than would be expected based on their stated uncertainty estimates. This lack of independence is not surprising as the algorithms use measurements from the same sensor (albeit not identical spectral bands) and make some similar algorithmic assumptions, but is important to state nonetheless, so that users are aware of it. As well as highlighting regions for further study and algorithmic refinement, for those areas where Figure 6 is shaded in red tones, it may be less critical to an end-user which of the two algorithms (DB or DT) they use for their particular scientific application, while for those shaded in blue tones, it is more likely that use of the different algorithms in an analysis may result in different conclusions being reached.

3.2. Comparison of Relative Sampling Rate

This section examines how spatial coverage differs between the two data sets for those areas where both attempt retrievals. Figure 7 shows the seasonal ratio of the number of available DB retrievals passing QA checks to the number of available DT retrievals passing QA checks, on a 1° grid, for those grid cells where both algorithms provide retrievals. Related to this, Figure 8 shows, for both algorithms, the fraction of attempted retrievals which pass QA checks. This is provided on an annual basis for brevity, as regional variation in this metric was found to be larger than seasonal variation.

These figures show that the coverage provided by the two algorithms can differ considerably (by a factor of 3 or more) on both a regional and seasonal basis. Overall, DB provides more retrievals over many parts of the world, particularly those which are seasonally semiarid. In contrast, DT provides significantly more retrievals over tropical rainforests and southern Asia in JJA. The ratio of the number of retrievals is otherwise close to unity in southern Asia in other seasons, over large parts of South America outside of the Amazon and Andes, and over selected regions of North America and Eurasia on a seasonal basis. Figure 8 suggests that these differences are explained not just by choice of pixels to use in retrieval (i.e., DT only retrieving over scenes deemed sufficiently dark) but also large part by QA checks in the retrievals. In particular, DB assigns "good" QA values less often than DT in forested tropical regions, where cloud cover is frequently dominated by small broken cumulus cloud fields. Figure 9 provides an example of this over the Amazon; prior to QA checks DB and DT obtain similar coverage but filtering out poor-QA retrievals (QA≤1 for DB, QA≤2 for DT, QA=0 for ocean) removes a significantly higher amount of DB retrievals in the gaps between cumulus

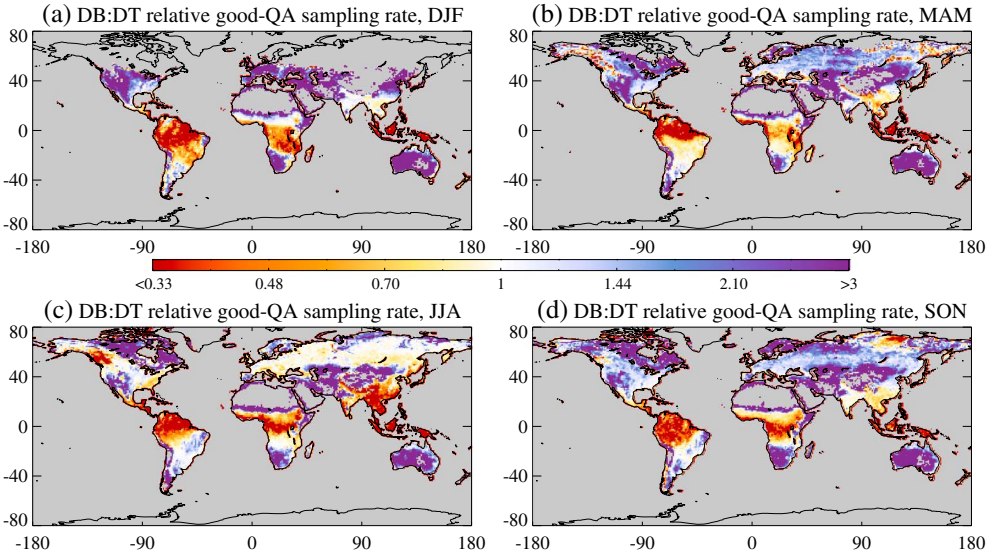

Figure 7. Seasonal ratio of the number of DB retrievals passing QA checks to the number of DT retrievals passing QA checks, for (a) DJF, (b) MAM, (c) JJA, and (d) SON. Grid cells where one or both algorithms provide fewer than 10 retrievals passing QA checks in a season are shaded in grey.

clouds. Conversely, DB assigns good-QA more frequently in many sparsely vegetated regions. Figure 10 provides an example over Europe, where retrieval coverage of DB and DT is similar (aside from an arid portion of Spain). Although not directly relevant to DB/DT comparisons due to an absence of coverage of one of the algorithms, good QA is almost always assigned over oceans and by DB over deserts (Figure 8).

3.3. Aggregated Pixel-Level Data

As before, the results in this section were obtained by considering only those pixels where both DB and DT algorithms provided a retrieval passing QA checks, although only every 10th day during the years 2006–2008 were used (6,692,616 pairs of matched retrievals) for a more manageable data volume.

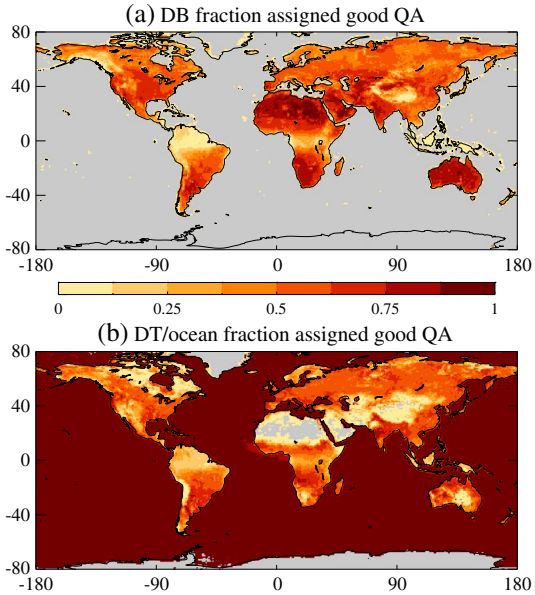

Figure 8. Fraction of attempted retrievals passing QA checks, for (a) Deep Blue and (b) Dark Target land/ocean. Grid cells where the algorithm in question provides fewer than 10 retrievals are shaded in grey.

Figure 11 shows binned statistics of retrieved AOD and the difference $\tau_{DB} - \tau_{DT}$. Figure 11a shows a peak in retrieved AOD near 0.1 and a rapid decline in frequency of occurrence as AOD increases to about 1, in both DB and DT. Outside of this range, some key differences become more apparent. Firstly, DT permits retrieval of small negative AOD (down to −0.05) which, while unphysical, are retained as an attempt to ensure that AOD in clean conditions does not have biases truncated in one direction. This happens in approximately 20% of pixels in the matched set and occurs most frequently over Australia in all seasons and over eastern Brazil in JJA. DB does not permit retrieval of negative AOD. This algorithmic difference explains, in part, the lower correlation of DB and DT in these regions shown in Figure 5 and the lower frequency of agreement in these regions shown in Figure 6.

Secondly, the maximum permitted AOD in DT is 5; in DB the limit is lower (as mentioned, AOD retrieval is performed individually at a combination of 412, 470, and 650 nm, each of which is capped at an AOD of 3.5 at that wavelength,

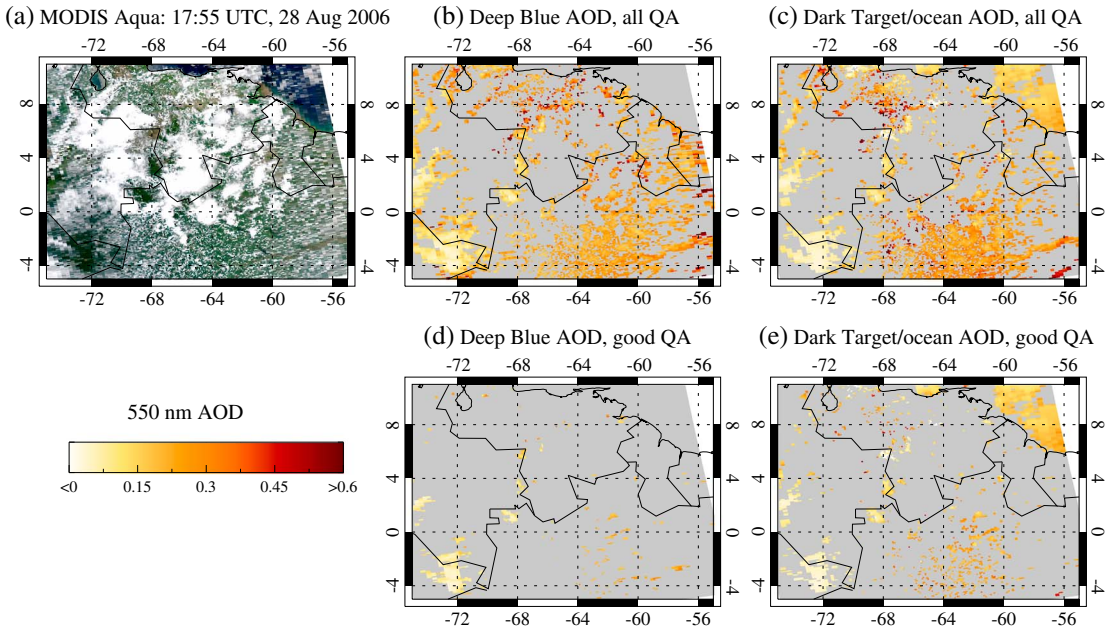

Figure 9. Example of QA filtering for a MODIS Aqua granule over the Amazon. (a) A true-color image. (b and c) DB and DT land/ocean AOD, respectively, without QA filtering. (d and e) The same after data are filtered to remove those pixels failing QA tests. Regions in grey lack valid AOD retrievals.

and then interpolated to 550 nm). These extreme high values of AOD are rarely encountered (fewer than 5% of retrievals in either data set are for AOD above 1) but can influence the regional statistics. DB AOD tends to be lower than DT in the high-AOD region of China throughout the year and in the main South American biomass burning season (SON). Overall, the mean and median AOD from DB for this matched set of retrievals are 0.156 and 0.086, respectively, and for DT 0.142 and 0.077, respectively, while the standard deviations are 0.197 for DB and 0.225 for DT. The lower median than mean AOD in both cases is a result of the well-known tendency for AOD distributions to be approximately lognormal [e.g., *O'Neill et al.*, 2000]. The slightly lower median/mean and higher standard deviation in DT as compared to DB reflects the ~20% of retrievals where $-0.05 \leq \tau_{DT} \leq 0$.

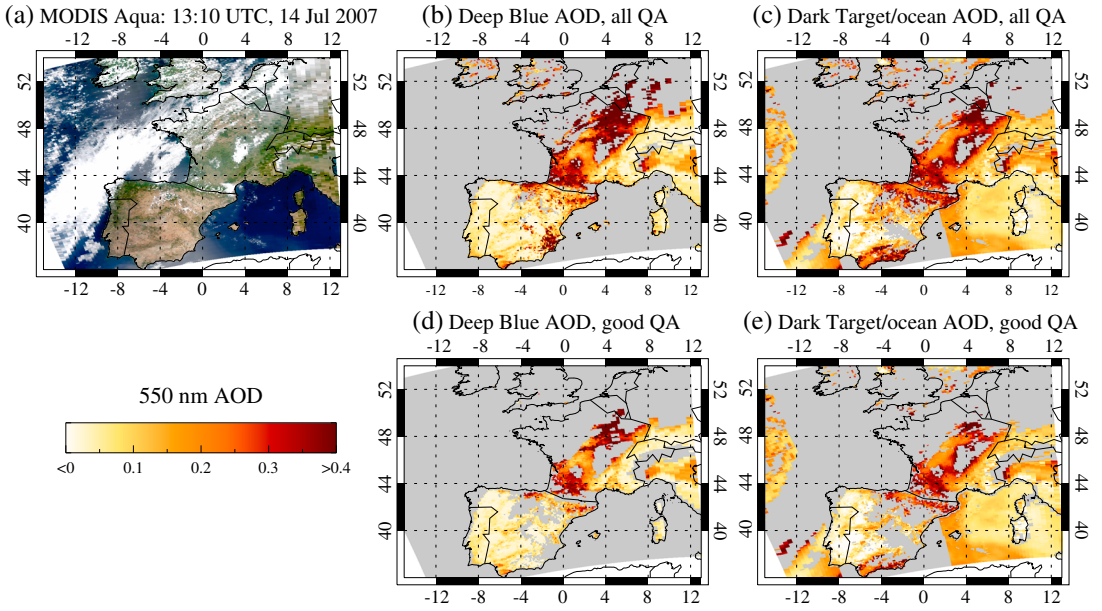

Figure 10. As Figure 9, but for a granule over Europe.

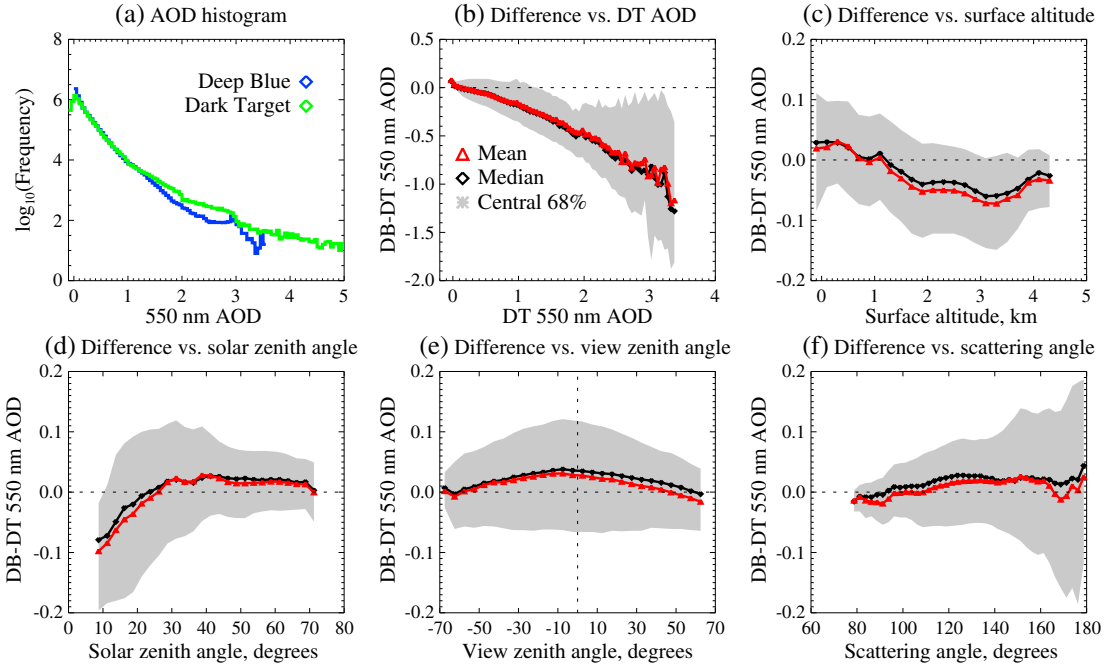

Figure 11. Comparative statistics of Deep Blue/Dark Target AOD retrievals. (a) Histograms of retrieved AOD, with a logarithmic frequency scale. (b–f) The difference ($\tau_{DB} - \tau_{DT}$) binned as a function of τ_{DT}, surface altitude, solar zenith angle, view zenith angle, and scattering angle, respectively. In Figures 11b–11f), red indicates bin mean values, black bin medians, and the central 68% range of the data is shown in grey.

These differences in extrema (on both ends) are also responsible in part for the positive offset (at near-zero AOD) and then increasingly negative $\tau_{DB} - \tau_{DT}$ as τ_{DT} increases in Figure 11b, although for the bulk of the data the overall bias is near-zero. Specifically, the 90th percentile of AOD is 0.38 in both data sets, and mean and median values of $\tau_{DB} - \tau_{DT}$ range from 0.02 (for $\tau_{DT} = 0$) to −0.005 (for $\tau_{DT} = 0.5$).

The remaining panels illustrate the elevation and angular dependence of $\tau_{DB} - \tau_{DT}$. As surface elevation increases, $\tau_{DB} - \tau_{DT}$ goes from positive to negative, likely as a result of differences in radiative transfer assumptions about the effects of elevation and surface pressure, and/or assumptions concerning surface reflectance. In particular, highly elevated surfaces are likely to be less densely vegetated (or vegetated in a different manner) than those near the surface and so it is possible that the algorithms' surface reflectance parameterizations are less valid in these situations. Studies have suggested that at high elevations, C5 DT data could be on average biased high [*Levy et al.*, 2010; *Zelazowski et al.*, 2011] and C6 DB data on average biased low [*Sayer et al.*, 2013], which is consistent with these results. However, for the bulk of the data (the 90th percentile of surface altitude is 1.23 km), the difference and its variation with altitude are small.

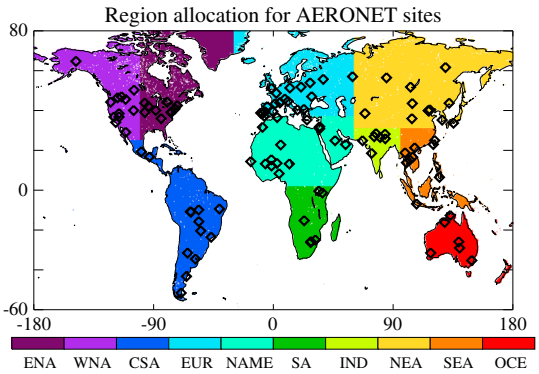

Figure 12. Geographical bounds of regions used in this study for grouping of MODIS and AERONET AOD. Locations of the AERONET sites used are indicated by black diamonds. Region names and associated abbreviations are Eastern North America (ENA), Western North America (WNA), Central/South America (CSA), Eurasia (EUR), North Africa/Middle East (NAME), Southern Africa (SA), Indian subcontinent (IND), North-East Asia (NEA), South-East Asia (SEA), and Oceania (OCE).

Figures 11d–11f reveal some interesting angular dependencies. While there is near-zero average difference at the edges of the swath, near the center DB is higher than DT by about 0.03, and the peak of this difference is found around 10° viewing zenith angle on the western side of the swath. The reasons for this are unclear. A similar offset is found at many solar zenith and scattering angles, although for high-Sun conditions $\tau_{DB} - \tau_{DT}$ can become as low as −0.1 on

average. It is possible that this is related to the fact that these geometries tend to be encountered in the tropics during the summertime, in which AOD tends to be high (as a result of dust/smoke), and so this may be in part a result of the AOD-dependence of $\tau_{DB} - \tau_{DT}$ (Figures 11a and 11b) rather than anything directly related to solar zenith angle. The distribution of $\tau_{DB} - \tau_{DT}$ also becomes broader at angles near backscatter, which may be related to difficulties modelling the surface BRDF hot spot [*Hyer et al.*, 2011; *Sayer et al.*, 2013]. Backscatter geometries and low solar zenith angles are also associated with higher DB retrieval uncertainty, which is reflected in the uncertainty estimates provided within the C6 data files [*Sayer et al.*, 2013].

The difference $\tau_{DB} - \tau_{DT}$ was also examined as a function of fractional cloud cover (as estimated by the DT retrieval cloud mask) within the retrieval pixel, stratified by solar/view geometry and land surface cover. These results are omitted for brevity; no strong dependence of $\tau_{DB} - \tau_{DT}$ on cloud cover or proximity was found. This does not imply that there is no bias in either product with increasing cloud fraction but rather that any biases are likely similar.

4. Comparison Against AERONET

4.1. AERONET Data and Matchup Protocol

The Sun photometers used by AERONET derive total columnar spectral AOD with low uncertainty (~0.01–0.02), much smaller than typical satellite uncertainties, through observation of direct solar radiation and subsequent correction for the scattering and absorption of gases in the atmosphere [*Holben et al.*, 1998]. Almost all AERONET sites provide AOD at 440, 675, 870, and 1020 nm, and many provide data at additional wavelengths. Under cloud-free conditions, observations are taken at fairly high temporal resolution (~15 min). Due to this low uncertainty and standardisation of network protocols across sites in a wide range of locations (several hundred at the time of writing), AERONET direct-Sun data have been used for multiple purposes, including the large-scale validation and bias-correction of satellite AOD for many different data sets [e.g., *Ichoku et al.*, 2002; *Zhang and Reid*, 2006; *Levy et al.*, 2010; *Kahn et al.*, 2010; *Bréon et al.*, 2011; *Hyer et al.*, 2011; *Sayer et al.*, 2012b, 2013].

The recommended AERONET data product for most quantitative applications is known as Level 2.0, which has undergone cloud screening, calibration checks, and quality assurance [*Smirnov et al.*, 2000]; the current Version 2 of this product is used here. A total of 111 sites are used, shown in Figure 12, corresponding to the 60 sites considered by *Sayer et al.* [2013] when validating the C6 DB data, plus an additional 51 sites chosen primarily because of their good data volumes, and to expand coverage of some regime types (e.g., the Indian subcontinent and south-eastern Asia, and some elevated areas).

The sampling strategies of AERONET and satellite sensors are quite different, and as such a direct comparison between the two is nearly impossible: AERONET provides repeated point measurements of the aerosol column between Sun and ground site, while satellites provide an instantaneous snapshot of the aerosol column between ground and sensor, across a swath. Thus, this study follows the widely used protocol (e.g., prior references) of averaging AERONET data around the time of the satellite overpass (here, ±30 min), and averaging satellite data (passing QA checks) spatially near the AERONET site (here, ±25 km), to mitigate the effect of variability in the underlying aerosol field on the comparison. The AERONET AOD at 550 nm (τ_A) is obtained by interpolating the spectrally closest AERONET AOD (normally 440 or 500 nm) using the standard Ångström exponent α. As AOD tends to vary smoothly through this spectral region, typically negligible (<0.01) uncertainty is introduced by this interpolation. A valid matchup is obtained when there is at least one MODIS retrieval passing QA checks near the site and at least one AERONET observation near the time of the satellite overpass. Although averaging the satellite data rather than requiring an exact pixel-level matchup may decrease the apparent level of random error, in practice for these algorithms the statistical difference has been found to be, in most cases, negligible and smaller than site-to-site or algorithm-to-algorithm variability [*Petrenko et al.*, 2012; *Sayer et al.*, 2012b], due in part to small sensor noise. Additionally, the spatial averaging provides a significantly larger data volume for analysis.

4.2. AERONET Comparisons and Evaluation Metrics

The C6 DB AOD was validated by *Sayer et al.* [2013]; some DT validation results were presented by *Levy et al.* [2013]. Thus, the analysis here focusses more on the comparative performance of DB, DT, and the merged SDS on a global and regional (regions defined in Figure 12) basis, with the intent that this will aid users in understanding the characteristics of the various MODIS aerosol products for their particular region(s) of study, and provide direction for future evaluation/improvement studies of these data products. Two sets

Table 2. Global and Regional Statistics of MODIS/AERONET Comparison of AOD at 550 nm, for the Data Collocated on an Individual MODIS Retrieval-Level[a]

Region	Number of Sites	Number of Matches	*R*			Median Bias			*f* Within EE_{DT}			RMS Error		
			DB	DT	Merge	DB	DT	Merge	DB	DT	Merge	DB	DT	Merge
Global	111	49039	**0.89**	**0.89**	**0.89**	−0.017	**−0.011**	−0.014	**0.76**	0.67	0.69	**0.11**	**0.11**	**0.11**
ENA	10	5205	0.86	**0.88**	**0.88**	**0.0017**	−0.0035	−0.0030	**0.87**	0.76	0.77	**0.055**	0.069	0.069
WNA	12	6251	0.74	0.70	**0.77**	**−0.012**	0.023	**0.012**	**0.81**	0.69	0.76	**0.078**	0.11	0.095
CSA	13	4527	0.89	**0.92**	**0.92**	**−0.028**	−0.049	−0.049	**0.72**	0.51	0.54	0.12	**0.11**	**0.11**
EUR	21	14252	**0.87**	0.86	0.86	−0.015	**−0.0099**	**−0.0099**	**0.83**	0.74	0.74	**0.067**	0.081	0.080
NAME	15	4402	0.80	0.81	**0.82**	−0.036	**−0.013**	−0.029	0.54	**0.60**	**0.60**	0.18	**0.17**	**0.17**
SA	6	2197	**0.89**	0.81	0.82	**−0.031**	−0.056	−0.057	**0.74**	0.55	0.54	**0.078**	0.11	0.11
IND	7	2777	0.85	**0.87**	0.86	−0.073	**−0.014**	−0.025	0.60	**0.71**	0.69	0.17	**0.15**	0.16
NEA	12	4351	0.93	**0.94**	**0.94**	−0.025	**0.0016**	−0.0043	0.69	0.70	**0.72**	**0.14**	0.15	**0.14**
SEA	9	2038	0.84	**0.88**	**0.88**	**−0.0013**	−0.010	−0.010	**0.62**	0.56	0.56	0.17	**0.15**	**0.15**
OCE	6	3039	**0.67**	0.64	0.64	**−0.018**	−0.044	−0.042	**0.85**	0.62	0.64	**0.073**	0.088	0.088

[a]Regions are defined in Figure 12. In each row, the best performing of the three algorithms by each metric is indicated in bold.

of MODIS/AERONET comparisons are presented herein: firstly, looking at only those 10 km×10 km pixels where all three SDSs (DB, DT, and the merge) provide retrievals passing QA checks, and secondly, validating the three SDSs independently (i.e., not requiring such pixel-level collocation between the three). These are referred to as the "collocated" and "all matches" cases, and global and regional statistics are presented in Tables 2 and 3, respectively. The "collocated" set is useful for comparing contextual biases in the data sets (related to, e.g., assumptions related to surface/aerosol properties), as there is a direct correspondence in the individual retrievals from both algorithms included, while the "all matches" set provides an evaluation of a single algorithm distinct from the others.

The statistical metrics considered in the evaluation are *n*, the number of MODIS/AERONET matchups; *R*, the linear correlation coefficient; the median bias (defined such that positive values indicate a MODIS overestimate); the root mean square error (RMSE); and *f*, the fraction of MODIS/AERONET in agreement within the DT algorithm's expected uncertainty $EE_{DT}=\pm(0.05+0.15\tau_A)$. Although DB and DT have different expected uncertainties, presenting statistics here in terms of EE_{DT} (which is defined relative to AERONET and so is independent of the MODIS data) allows the performance of DB, DT, and the merged SDS to be compared with each other more directly. Statistics of AERONET comparisons for individual sites are omitted for brevity but available from the authors on request.

4.3. Site-Level Versus Regional-Level Analyses

A difficulty with aggregated global/regional statistics is the inhomogeneity of AERONET site locations across the globe (or within a region) and the differences in data volume between sites, meaning that sites are not weighted equally in combined metrics. Figure 13 presents histograms of differences in validation statistics from the "collocated" comparison for the 102 sites (out of 111) where at least 25 (three-way DB/DT/merged) matchups were found. The remaining nine sites are in arid/semiarid areas where DT provides zero or few retrievals. The threshold of 25 is an attempt to provide some statistical robustness, although broad features are similar for other thresholds. Differences in R^2 are presented rather than differences in *R*, to better reflect

Table 3. As Table 2, Except for the Three Data Sets Validated Independently (i.e., Not Requiring Pixel-Level Collocation)

Region	Number of sites	Number of Matches			*R*			Median Bias			*f* Within EE_{DT}			RMS Error		
		DB	DT	Merge	DB	DT	Merge	DB	DT	Merge	DB	DT	Merge	DB	DT	Merge
Global	111	80125	59161	**81636**	**0.89**	**0.89**	0.88	−0.0098	**−0.0040**	−0.0047	**0.72**	0.66	0.65	0.13	**0.12**	0.13
ENA	10	**6909**	5972	6530	0.80	**0.89**	0.88	0.0082	**0.0012**	0.0044	**0.82**	0.74	0.75	**0.066**	0.079	0.080
WNA	12	9632	7015	**9662**	0.81	**0.82**	0.81	**-0.0056**	0.029	0.0098	**0.80**	0.65	0.75	**0.096**	0.12	0.11
CSA	13	5578	5936	**6311**	0.90	**0.91**	0.90	**−0.022**	−0.033	−0.032	**0.73**	0.54	0.56	**0.14**	**0.14**	**0.14**
EUR	21	**18630**	17077	17570	**0.85**	**0.85**	**0.85**	−0.011	−0.0067	**−0.0062**	**0.83**	0.73	0.73	**0.071**	0.082	0.082
NAME	15	16629	5578	**17245**	**0.86**	0.80	0.85	−0.0059	0.00075	**0.000053**	0.55	**0.57**	0.55	**0.17**	**0.17**	**0.17**
SA	6	2419	2993	**3083**	**0.89**	0.78	0.79	**−0.032**	−0.041	−0.044	**0.73**	0.58	0.57	**0.080**	0.10	0.10
IND	7	4250	3034	**4326**	0.84	**0.86**	0.83	−0.091	**−0.0070**	−0.056	0.51	**0.70**	0.57	0.20	**0.17**	0.20
NEA	12	8075	5240	**8117**	0.92	**0.93**	**0.93**	−0.013	0.013	**0.0031**	0.66	**0.68**	0.67	0.17	**0.15**	0.16
SEA	9	2231	2763	**2764**	0.81	**0.87**	**0.87**	**0.0068**	0.035	0.035	**0.61**	0.51	0.52	0.19	**0.17**	**0.17**
OCE	6	5772	3553	**6028**	0.56	**0.63**	0.54	**−0.0054**	−0.036	**−0.012**	**0.82**	0.65	0.71	**0.070**	0.086	0.079

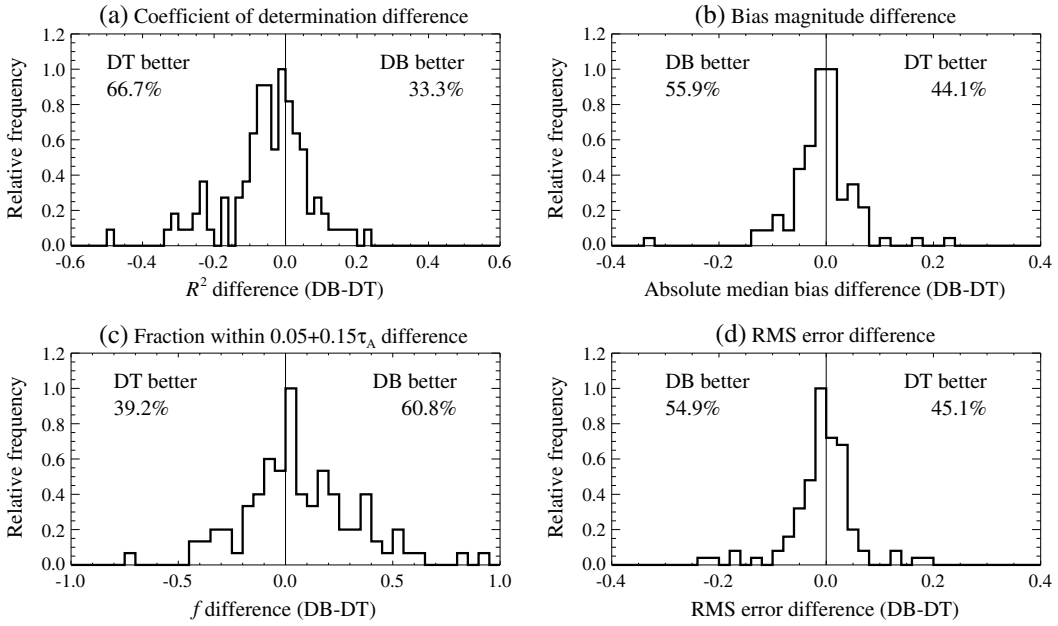

Figure 13. Histograms of (DB−DT) differences in validation statistics across the ensembles of validation sites used, for the 102 sites with at least 25 data points. Difference statistics are presented for (a) R^2, (b) absolute value of median bias, (c) f, and (d) RMS error. For each metric, the fraction of sites where each algorithm performs best is indicated toward the upper left/right of the plot.

the difference in the algorithms to track variability in AOD, and that the difference in absolute bias is presented rather than the difference in bias itself (as a "better" comparison will have a bias closer to zero, and not necessarily more positive or negative).

DT has a higher R^2 at ~67% of sites, while DB performs better at ~60% of sites in terms of f, and ~55% in terms of bias and RMS error. The absolute differences in all these metrics are often (but not always) not large, suggesting that the quality of both algorithms is frequently similar for a given site. If the "all points" rather than "collocated" matchups are used, quantitatively similar results are obtained.

It is important to recall that the AERONET validation only allows inference about performance of the retrieval as a whole by analysing the small sample of retrievals near a given site which have a matchup, from the total population of retrievals near that site. Site-level analysis is not a main focus of this study due in part to small sample sizes leading to difficulty in determining the true population performance of DB and DT at sites robustly from the available smaller sample performance (i.e., difficulties inherent in inferring broader-scale performance from the sample of points where matchups with AERONET are obtained). For example, for two correlated variables (here τ_A and τ_M) sample correlation coefficients (here, R) converge to the underlying true population correlation coefficient as sample size tends to infinity, but for smaller samples, the estimate of the true correlation coefficient is more uncertain. For a population of paired data with a true correlation coefficient of 0.7 (common at some AERONET sites), 129 data points are required to estimate R within ±0.1 (i.e., the confidence range 0.6–0.8) for a single data set with 95% confidence [*Schonbrödt and Perugini*, 2013]. Determining the sign of the difference between the two algorithms' true correlation coefficients is correspondingly more difficult. Hence, as differences between DB and DT R against AERONET at an individual site are often 0.05 or smaller, it is often not possible to infer robustly which algorithm is performing better for an individual site. Thus, upscaling to regional analysis and/or stratification of data by other means (e.g., with respect to surface or aerosol properties) are advantageous to infer retrieval performance more robustly. The same argument also applies to the other statistical metrics.

5. Discussion and Usage Recommendations

5.1. Dependence of Retrieval Error on Surface Cover

The DT algorithm parametrises surface reflectance based on a swIR NDVI, hereafter $NDVI_{sw}$, defined $(\rho_{1.24} - \rho_{2.12})/(\rho_{1.24} - \rho_{2.12})$, where $\rho_{1.24}$ and $\rho_{2.12}$ indicate TOA reflectance corrected for gaseous absorption at the

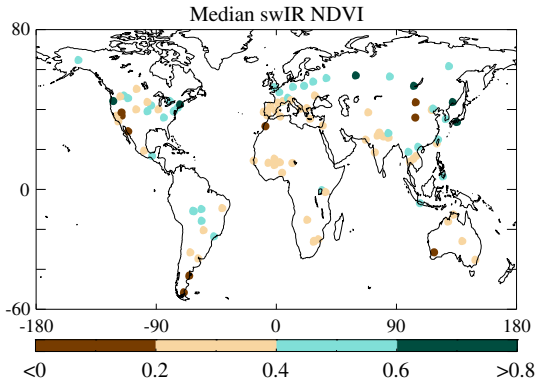

Figure 14. Median $NDVI_{sw}$ for each AERONET site, from the "collocated" set of DB/DT/AERONET matchups.

MODIS bands centred near 1.24 and 2.12 µm, respectively [*Levy et al.*, 2007]. Like the standard (red/nIR) NDVI, more positive values of $NDVI_{sw}$ tend to be associated with increased cover of green vegetation, although the longer wavelengths used mean that $NDVI_{sw}$ is less strongly affected by atmospheric scattering/absorption [*Karnieli et al.*, 2001]. The median $NDVI_{sw}$ observed at each site for the "collocated" set of matchups is shown in Figure 14. Permanently arid sites, particularly in elevated terrain, tend to have $NDVI_{sw} < 0.2$, while other arid sites and sites with seasonal variations in extent of vegetation often lie in the region $0.2 < NDVI_{sw} < 0.4$. Higher values are associated with more densely vegetated sites, with the maximum value observed around 0.8.

Analysing dependence of AOD error on $NDVI_{sw}$ in conditions of low aerosol loading provides a comparison of DB/DT performance for those cases where the relative contribution to total uncertainty arising from surface reflectance assumptions is highest, using $NDVI_{sw}$ as a proxy for surface type. Figure 15 shows the distribution of DB and DT retrieval error as a function of $NDVI_{sw}$, for low-AOD conditions ($\tau_A < 0.2$; 33,321 points, corresponding to 68% of the "collocated" data set). DB shows little dependence of error (in terms of median bias, or spread of the error), while the pattern for DT is more complicated. The data can be divided into four regimes with different attributes, over the following approximate ranges of $NDVI_{sw}$:

1. $NDVI_{sw} < 0.2$. For the lowest $NDVI_{sw}$, the DT median bias is positive, gradually becoming negative (from 0.03 to −0.04) as $NDVI_{sw}$ increases, while the DB median bias is more stable (changing from 0 to −0.02). The DB data are also much more tightly clustered around this median bias than DT.
2. $0.2 < NDVI_{sw} < 0.4$. Here DB and DT biases are both fairly stable, around −0.01 for DB and −0.03 for DT. The difference (DB higher by 0.02) corresponds to the typical offset observed between the two over many partly vegetated regions (e.g., Figure 4). The spread of DB data is narrower than for DT.
3. $0.4 < NDVI_{sw} < 0.6$. Here DB and DT have a very similar median bias of order 0 to −0.01. The negative tails of the error distributions are similar, although DT has a larger positive tail (i.e., is slightly more prone to high-biased outliers). Overall, the error characteristics of DB and DT are similar in this range.
4. $NDVI_{sw} > 0.6$. For the highest $NDVI_{sw}$, the DB median bias becomes increasingly negative (down to −0.03) while the DT median bias remains comparatively closer to zero. Both algorithms' spreads of retrieval error narrow down.

Error statistics for DB, DT, and the merge in this low-AOD regime are tabulated in Table 4. The merge slightly outperforms DB and DT in terms of correlation ($R = 0.58$ as compared to 0.55 and 0.54, respectively). The low correlation in all cases is a result of the fact that, by restricting to low-AERONET AOD conditions, the dynamic range of "true" AOD is small and the retrieval uncertainty comparatively large. For all algorithms, the fraction matching AERONET within EE_{DT} is substantially higher than the "target" value of 68%; DB has the best performance by this metric. This suggests that DT performs better than its stated global-average uncertainty in these conditions, which may therefore be revised to be more narrow. Note that DB is also evaluated relative to the DT error metric to permit a direct comparison here; however, the DB uncertainty estimate as provided within the data set [*Sayer et al.*, 2013] drops to ~0.03 in the lowest-AOD conditions, compared to 0.05 for DT, which is consistent with these results (i.e., smaller errors in low-AOD conditions for DB compared to DT). DB also has a slightly lower RMS error (0.062) than DT (0.077) and the merge (0.071) in these conditions.

For $\tau_A > 0.4$ (not shown), these patterns no longer hold, with no dependence of error on $NDVI_{sw}$. The higher AOD means that assumptions about aerosol optical properties become comparatively more important to determining the total retrieval error. The presence of aerosols in the atmosphere also acts to blur spectral contrast in TOA reflectance measurements such that the dynamic range of $NDVI_{sw}$ is smaller.

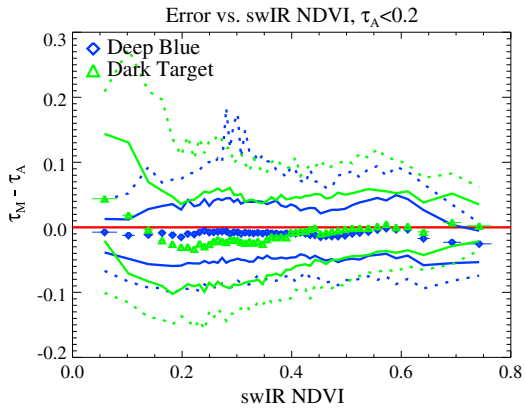

Figure 15. Error in MODIS AOD as a function of $NDVI_{sw}$, for low-AOD conditions (τ_A<0.2), from the "collocated" set of DB/DT/AERONET matchups. DB data are shown in blue and DT in green. Symbols show the median error (and horizontal lines the standard deviation of $NDVI_{sw}$ in each bin, for a total of 50 evenly populated bins). Solid colored lines indicate the central 68% of the data, and dashed colored lines the central 90%. The line of zero difference is shown in red.

5.2. Dependence of Retrieval Error on Aerosol Properties

The chief parameters determining the magnitude and spectral dependence of the aerosol contribution to TOA reflectance through the visible and swIR wavelength range are the total AOD, particle size, and SSA. The DB and DT algorithms use different aerosol optical models, and in the absence of correlative ground-truth information on a case-by-case basis, it is impractical within the scope of this study to exhaustively examine each of these factors on a regional basis, particularly as the algorithms also use some different MODIS bands. What is more practical and readily available is to use AERONET α (determined over the wavelength range 440-870 nm) as a first-order indicator of the optical dominance of fine-mode or coarse-mode aerosols within an atmospheric column [e.g., *Eck et al.*, 1999], to make some generalisations about algorithm performance for fine/coarse-dominated aerosols in high-AOD regimes.

This is presented in Figure 16, for τ_A >0.4 from the "collocated" set of matchups, for the three cases of α <0.7 (1228 points; aerosol likely dominated by mineral dust); 0.7< α <1.3 (1620 points; aerosol likely a mixture of fine- and coarse-mode aerosols, or fine mode dominated under conditions of high humidity) and α >1.3 (2973 points; aerosol likely dominated by small particles such as smoke or industrial pollution).

For dust-dominated cases (α <0.7), DB has a fairly AOD-independent median bias around −0.15 while the DT median bias is closer to zero but becomes more negative with increasing AOD (to −0.35 at τ_A ~1.4). The DB data show a narrower spread of error throughout. For mixed aerosols (0.7< α <1.3), the DT bias is persistently closer to zero while the DB bias is similar to the dust-dominated case, and the DB error spread is again narrower. Thus, a user's preferred data set for analysis of these conditions may be dependent on whether overall bias or absolute uncertainty is more important. For fine-mode-dominated aerosols (α >1.3), DT has very little median bias while the DB bias is slightly more negative than in the other two aerosol regimes; the spread of uncertainty envelopes is similar for the two algorithms.

Error statistics for DB, DT, and the merge in these high-AOD regimes are tabulated in Table 4. The RMS error is similar in all three data sets, for a given AOD/α stratification. Biases tend to be negative, and DT biases tend to be least negative. DB has highest correlation of the three for the low and moderate α groupings (dust-dominated and mixed aerosols), but lowest fraction matching within EE_{DT}. Note that because of the requirement for all three data sets containing valid retrievals, this analysis excludes dust over bright deserts, where DB is the only algorithm providing data. For fine-mode dominant aerosols (α >1.3), the situation is reversed, with DT and the merge having the highest correlation but DB the most points matching AERONET within EE_{DT}.

Table 4. Statistics of MODIS/AERONET Comparison of AOD at 550 nm, for the Data Collocated on an Individual MODIS Retrieval-Level, Stratified by AERONET Aerosol Characteristics[a]

Region	Number of Matches	*R*			Median Bias			*f* Within EE_{DT}			RMS Error		
		DB	DT	Merge	DB	DT	Merge	DB	DT	Merge	DB	DT	Merge
τ_A < 0.2	33321	0.55	0.54	**0.58**	**−0.010**	**−0.010**	−0.012	**0.84**	0.70	0.72	**0.062**	0.077	0.071
τ_A > 0.4, α < 0.7	1228	**0.83**	0.77	0.78	−0.16	**−0.095**	−0.13	0.43	**0.49**	0.44	**0.28**	**0.28**	**0.28**
τ_A > 0.4, 0.7 < α < 1.3	1620	**0.87**	0.84	0.84	−0.10	**−0.025**	−0.037	0.57	**0.59**	0.58	**0.22**	0.24	0.24
τ_A > 0.4, 1.3 < α	2973	0.79	**0.83**	**0.83**	−0.072	**−0.00079**	−0.0020	**0.62**	0.58	0.58	0.22	**0.21**	**0.21**

[a]In each row, the best performing of the three algorithms by each metric is indicated in bold.

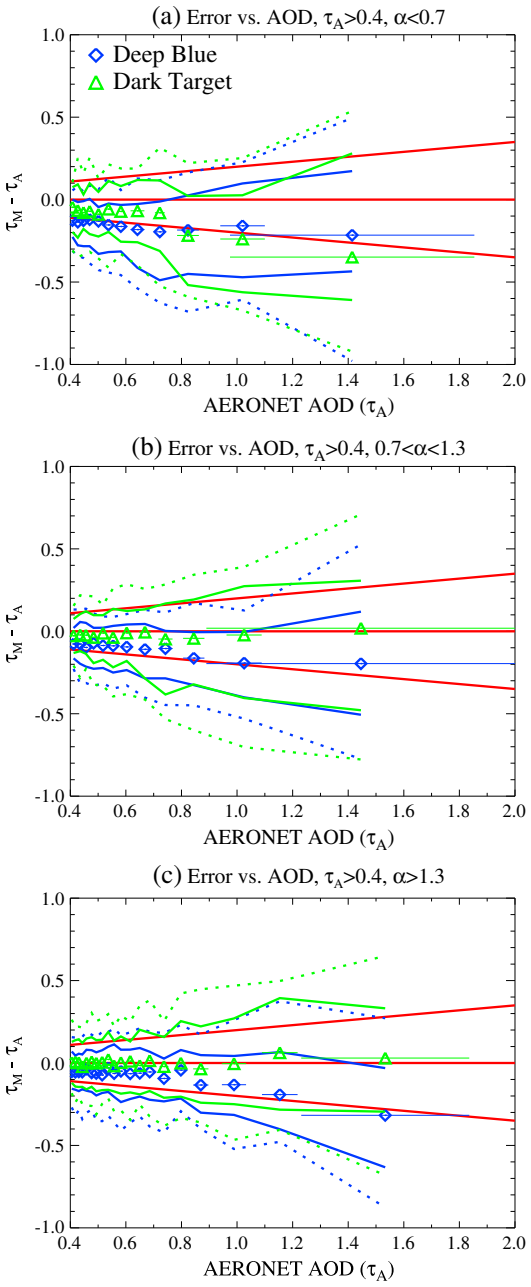

Figure 16. As Figure 15, except binned as a function of τ_A for high-AOD conditions (τ_A >0.4) and (a) α <0.7, (b) 0.7< α <1.3, and (c) α >1.3. A total of 12 evenly populated bins are used in Figures 16a and 16b, and 20 for Figure 16c. Red lines indicate zero difference and $\pm(0.05+0.15\tau_A)$.

Although DB has (on median average) a more negative bias than DT in these high-AOD conditions, Figure 16 suggests that this trend reverses for the highest-AOD events in dust-dominated cases, while the negative DB-DT relative bias observed at the highest AODs (Figure 11) comes predominantly from mixed and fine-mode-dominated aerosol distributions. Unfortunately, comparatively poor sampling of regimes with extreme high values of AOD (the 99th percentile of τ_A for this set of matchups is 1.2) limits generalisations about performance which can be made for the most extreme events, which are better suited to individual case studies, and lie outside the scope of the present work.

In contrast to section 5.1, in high-AOD conditions the fraction of points matching AERONET within EE_{DT} is substantially lower than the "target" value of 68%. This suggests that DT performs more poorly than its stated uncertainty in these conditions, which may need to be made broader. Note that the DB uncertainty estimate as provided within the data set [*Sayer et al.*, 2013] tends to ~20% in the highest-AOD conditions, compared to 15% for DT. This is again consistent with these results for the low- and moderate-α points, i.e., larger errors in high-AOD conditions for DB compared to DT.

5.3. Dependence of Bias on Surface Altitude and Solar/View Geometry

As a counterpart to Figures 11c–11f, Figure 17 shows the median bias in DB, DT, and merged AOD as a function of surface altitude and solar/view geometry. Although sampling is very different (AERONET matchups rather than all retrievals), similar general tendencies are observed. Specifically, the negative DB-DT difference at high elevation is linked to a negative bias in DB AOD compared to AERONET (most pronounced for the few sites above 2 km), while DT oscillates between small positive and negative biases in this regime. The negative DB-DT difference for solar zenith angles smaller than 20° is linked to negative biases of DB, and positive biases of DT, relative to AERONET. Interestingly, the merged data set is unbiased on average here; the tropical areas at which these solar zenith angles are encountered are also the regions/seasons where the merged data set draws more frequently from both the DB and DT algorithms. Tendencies of median bias with respect to view zenith angle and scattering angle are small. The merged SDS is intermediate, although tends to be closer to DT, as in this subset of data the merged SDS draws more often from DT than DB.

5.4. Regional Discussions

The discussion in this section uses mainly the "all matches" set of MODIS-AERONET matchups to illustrate individual data sets' performance. However, a similarity in statistics between the "collocated" and "all matches" matchup sets, both on a global/regional level (Tables 2 and 3) and on a site-by-site basis (not

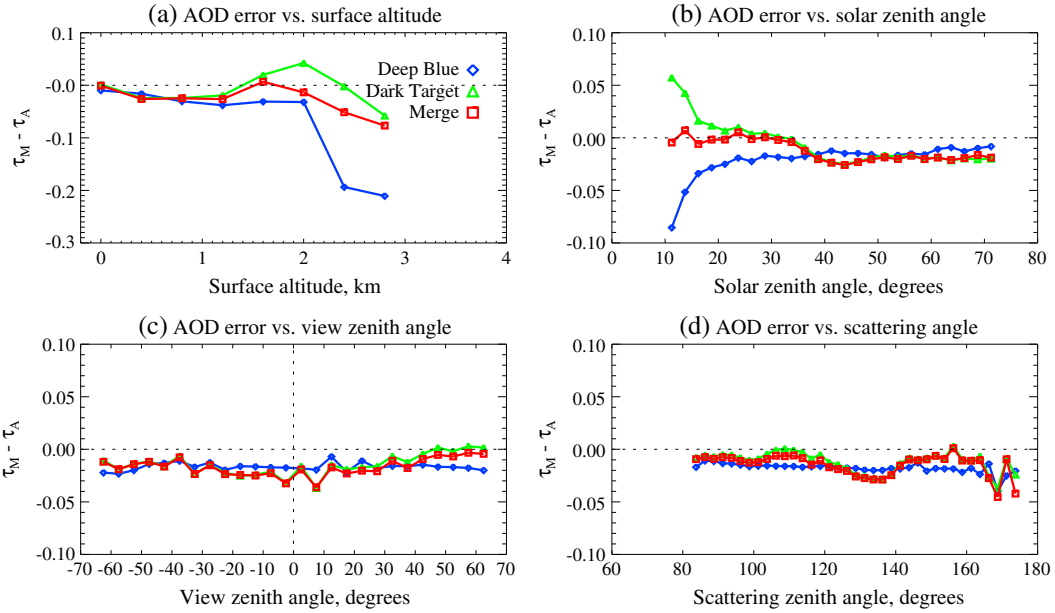

Figure 17. Median bias in MODIS AOD as a function of (a) surface altitude, (b) solar zenith angle, (c) view zenith angle, and (d) scattering angle, from the "collocated" set of DB/DT/AERONET matchups. DB data are shown with blue diamonds, DT with green triangles, and the merge with red squares. The line of zero difference is dashed.

shown), suggests that performance does not generally vary much between those cases where only DB or DT retrieves as compared to those cases where both do.

Figure 18 shows the "best" algorithm at each site according to various evaluation metrics (i.e., highest data volume, highest correlation, highest fraction matching within EE_{DT}, and lowest RMS error). Sites coloured golden brown (the category "merged is equal") indicate that the merged SDS and one of the other algorithms both perform equally superior to the other; examples include some desert regions (where the merge is completely DB and so by definition DB and the merge perform equally well) or some parts of the Amazon (where the merge is completely DT). The category "merged is superior," in contrast, indicates those sites where the merged SDS is superior to both DB and DT by the given metric, often due to seasonal variations

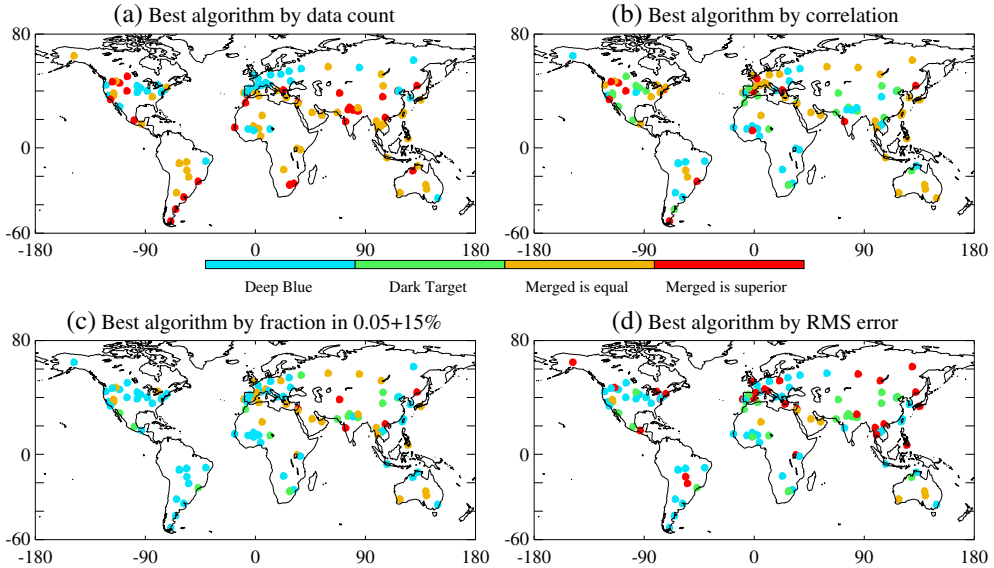

Figure 18. Maps showing the best performing of the MODIS aerosol SDS by different statistical metrics: (a) the data count, (b) correlation coefficient, (c) fraction of points matching AERONET within EE_{DT}, and (d) RMS error.

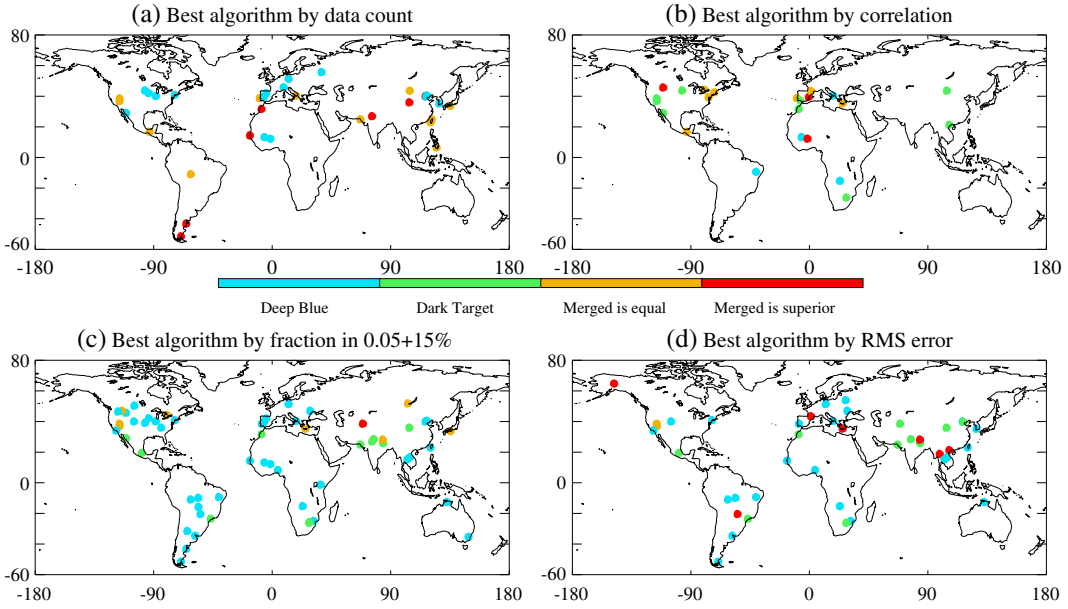

Figure 19. As Figure 18, except only for those sites where DB and DT both have at least 50 matchups with AERONET and performance differs by at least some threshold value: (a) 20% data count difference, (b) 0.1 difference in correlation coefficient, (c) 0.1 difference in fraction of points matching AERONET within EE_{DT}, and (d) 0.03 difference in RMS error.

in algorithm performance and seasonal variations in how the merged SDS is populated at a given site. Thus, for an ideal merging algorithm, each site and each metric would be colored a mixture of golden brown and red. Caution is advised in interpretation of this map, however, as the numerical difference in quality of the comparison is often small. Figure 19 provides a more quantitative view, by only showing sites where both algorithms provide at least 50 matchups with AERONET, and for a given metric, the DB and DT performance difference exceeds some threshold (20% in n, 0.1 in R, 0.1 in f, or 0.03 in RMS error, dependent on panel). This typically removes about half the sites for which DB and DT performance by that metric are similar and so facilitates identification of those sites for which one algorithm does perform significantly better by that metric.

Regional-scale statistics are provided as many users analyse MODIS aerosol data on a regional basis. Figures 18 and 19 reveal regional differences in performance between the algorithms but also differences between sites within individual regions. As is unsurprising based on the analysis so far, neither DB/DT nor the merged SDS consistently outperforms the others in all statistical metrics for all regions of the world. On a global basis, for both the "collocated" and "all matches" sets of matchups, DB has a larger fraction of matchups agreeing with AERONET within $\pm(0.05+0.15\tau_A)$, while DT and the merge have a median bias nearer to zero. Correlations are effectively identical. For the "all matches" analysis, the merged SDS provides about 1% more collocations with AERONET than DB; both provide about 35% more matchups on global aggregate than DT, in large part due to a lack of DT coverage in arid parts of (primarily) the NAME, NEA, and OCE regions. However, validation statistics are site-specific, as sections 5.1, 5.2, and 5.3 show the C6 data sets contain contextual errors, and regions are often not homogeneous in terms of aerosol or surface properties. Thus, although the comments below are framed in a regional context, data users are encouraged to bear the site-specific nature of validation in mind. Gaps in the validation network mean that the unknown retrieval quality in the absence of AERONET data must be inferred from similar regimes, which may not necessarily be in the same geographic region.

5.4.1. Coverage-Limited Areas

Figure 7 showed that in some areas the spatial coverage between the two algorithms is so different that it is likely to be the determining factor in which data set to choose. The most prominent such area is NAME; the bulk is desert surfaces which are too bright for the DT algorithm, and so DT coverage in NAME is largely restricted to several sites in the Sahel and Israel. The major aerosol type in NAME is wind-blown mineral dust, although over the Sahel contributions from biomass burning aerosols and industrial sources are also important [*Pandithurai et al.*, 2001; *Roberts et al.*, 2009]. As discussed by *Sayer et al.* [2013], DB performance

in this region is poorer than on global average, with an overall tendency to underestimate AOD, although performance has improved since C5. The correlation coefficient between DB and AERONET is high (0.86), indicating good ability to track changes in AOD. For the sites where both DB and DT provide retrievals, DB tends to perform better in the Sahel, while DT performs better at Nes Ziona (31.9°N, 34.8°E) and Forth Crete (35.3°N, 25.3°E). The merged SDS provides slightly poorer comparative statistics against AERONET than DB alone, indicating that those Sahelian sites for which the merged SDS draws from DT the quality of the data set is reduced. For applications in this region, from both retrieval coverage and quality points of view, DB seems the most appropriate choice. Other arid areas where DT coverage is limited or absent include deserts in central and eastern Asia, central Australia, parts of southern Africa and parts of Spain.

In tropical forested areas, DT coverage is significantly higher than DB, associated primarily with cloud/QA masking (section 3.2). This includes much of tropical South America and Africa, as well as the "Maritime Continent" (MC) in tropical Asia. Existing AERONET coverage is limited in all these areas. At the tropical African site of Mbita (0.4°S, 34.2°E), DT performs better than DB and provides a significantly higher data volume (443 compared to 48 matchups). Sites in the MC either have short (at present) data records or are in complex coastal environments where, combined with the high cloud cover, retrievals frequently are not attempted or fail [*Reid et al.*, 2013], and/or AERONET data may suffer from cloud contamination (e.g., the Singapore site; 1.3°N, 103.8°E) [*Chew et al.*, 2011]. The establishment of additional AERONET sites in the MC in recent years [e.g., *Salinas et al.*, 2013] should help pave the way for more robust estimates of retrieval performance. Recent and ongoing field campaigns such as AERONET's Distributed Regional Aerosol Gridded Observation Networks (DRAGON; http://aeronet.gsfc.nasa.gov/new_web/dragon.html) provide useful case studies in the MC and elsewhere. Analysis of C6 MODIS data during these campaigns is planned for the future, although out of the scope of the present study.

5.4.2. Dominantly Low-AOD Areas

Much of the regions ENA, WNA, and EUR, are characterised by typical $\tau_A \sim 0.1$–0.2 and vegetated, suburban, or urban surfaces over fairly flat, low-lying terrain, sampling periodic cases of transported aerosols such as wildfire smoke [e.g., *van der Werf et al.*, 2010] or transported mineral dust. As such in most cases the error characteristics of the retrievals are as discussed in section 5.1. In general for these sites DT has a slightly higher correlation with AERONET and smaller bias, while a higher fraction of DB matches agree with AERONET within EE_{DT}, and the RMS error of DB data is often slightly lower. The DB data volume is also often higher (Figure 7). However, at most sites in this category, performance of both algorithms is better than global average; coupled with the analysis in section 3, showing DB and DT provide very similar retrievals which are in agreement with each other more frequently than their global-average uncertainties would suggest, it is likely that any of the data sets would be suitable for quantitative scientific analyses in this region. These conditions are also found at some sites in southern CSA, and boreal parts of NEA.

Urban areas are also present in these regions, such as the CCNY site in New York City (48.2°N, 73.9°W). Here DB has a smaller median bias (0.025 vs. 0.083), RMS error (0.07 vs. 0.15), and higher fraction within EE_{DT} (0.76 vs. 0.42) than DT, along with a higher data volume. Urban terrain is known to pose a problem for the DT algorithm [e.g., *Levy et al.*, 2010; *Hyer et al.*, 2011], and work is underway to address this. DB does not exhibit obvious urban biases. The merged SDS mainly draws from DT at this site so is not optimal.

These regions also all contain semiarid and mountainous areas. Examples are provided by sites in WNA; at Frenchman Flat (36.9°N, 115.9°W) and Railroad Valley (38.5°N, 116.0°W), two sites in elevated semiarid regions of Nevada (USA), DT has a persistent high bias while DB retrieves a lower AOD (even in cases where AERONET AOD is high). The AERONET AOD is fairly persistently low; thus, DB matches more often within EE, although DT has higher correlation as it is better able to identify isolated extreme high-AOD events. At Rimrock (46.5°N, 117.0°W), a more vegetated area on the edge of the Rocky Mountains, both algorithms are in better agreement with AERONET.

OCE also falls into this category (note all sites considered are in Australia); AOD over Australia is typically <0.2, with high-AOD events mostly results of (local or transported) smoke from wildfires, and mineral dust [*Qin and Mitchell*, 2009]. Thus, many of the same comments apply. Over much of Australia, the terrain is arid and bright, such that only DB data are available; DT availability is largely confined to coastal regions and those areas where there is seasonal vegetation cover, such as Canberra (35.3°S, 149.1°E). Despite the differences in surface/aerosol conditions compared to the rest of the continent, statistics of the AERONET comparisons at Canberra largely mirror those of the region as a whole. DT often retrieves small positive or

negative AOD over much of Australia, such that DB performs better by most statistical metrics, consistent with the dependence of error on surface cover shown previously in section 5.1. The correlation coefficient for both algorithms is lower than in all other regions, reflecting the fact that AOD variability over much of Australia is often within retrieval uncertainty. The merged SDS offers performance approaching DB in quality and provides the highest data volume (by drawing on DT in the coastal regions, where DT provides better sampling). Unfortunately, the remoteness of much of the Australian continent means that large areas lack ground-truth data.

5.4.3. Dominantly High-AOD Areas

Several geographic regions contain sites with either seasonally or persistently high-AOD conditions. In CSA, the most well-known feature is the August–October peak biomass burning season [*van der Werf et al.*, 2010]; most matchups obtained with AERONET are from these seasons, due to high cloud cover at other times of year. Both algorithms have high correlation coefficients in the range 0.94–0.99, reflecting the large dynamic range of AOD at these sites (from near-zero up to ~4). In smoke-laden conditions, DB has a tendency to slightly underestimate AOD, while DT has a tendency to overestimate it. At each of these sites, approximately 25% more DB than DT matchups agree with AERONET within EE_{DT} (largely because of DT overestimates in high-AOD conditions); however, DT provides around 20% more matchups than DB (and a significant number more retrievals overall; Figure 7). CSA also contains sites in the urban areas of Mexico City (19.3°N, 99.2°W) and Tuxtla Gutierrez (16.8°N, 93.1°W). Both (particularly Mexico City) are situated in complex geographical and meteorological environments which can lead to the stagnation of polluted air above them [e.g., *Fast et al.*, 2007] with long high-AOD periods. DB and DT both underestimate AOD at these sites; DT performs better than DB and the merge, but statistical metrics are still poorer than global average.

Terrain in Southern Africa (SA) ranges from densely vegetated forests in the north through to croplands, grasslands, and desert in the south, much of it elevated. The main well-known aerosol signal from this region consists of smoke from biomass burning, although industrial sources are also important [*Piketh et al.*, 1999; *Roberts et al.*, 2009]. Seasonal variation in smoke aerosol composition has been shown to lead to seasonally varying biases in satellite-retrieved AOD [e.g., *Eck et al.*, 2013]. The merged SDS draws mostly from DT in this region, with dry-season contributions from DB in the southern and eastern edges, and DB always used over mountainous and desert areas (mostly in Namibia and western South Africa). Regional statistics are dominated by a large number of matchups at Mongu (15.2°S, 23.1°E) and Skukuza (25.0°S, 31.6°E), for which DB has a slightly lower data volume but otherwise significantly outperforms DT (smaller bias, RMS lower by ~40%, and about 30% more points in good agreement with AERONET). The merged SDS draws from DT over Mongu, and both algorithms over Skukuza, although not in an optimal way. DT performs better than DB (to differing extents, dependent on site and metric) at the other four sites considered in this region.

Both SEA and NEA are heterogeneous in terms of surface cover and aerosol type, with seasonally varying contributions from urban/industrial emissions, biomass burning, and mineral dust [*van der Werf et al.*, 2010; *Henriksson et al.*, 2011; *Gautam et al.*, 2013]. In NEA and SEA, the type dependence of retrieval error (section 5.2) means that the different algorithms may perform better or worse in different seasons and at different locations, due to the variety of aerosol type. The merged SDS may be most suitable for most regional-scale applications, as it provides the best coverage, although studies focussed near a single AERONET site may wish to use either (or both) DB or DT. At individual sites, DB data often give a better overall agreement with AERONET (in terms of matching within EE), although DT may represent AOD during extreme events more accurately.

The portion of southern Asia around the Indian subcontinent (IND) also fits in this category. The majority of AERONET sites used in IND are in or near the Indo-Gangetic Plain (IGP), with the exception of Pune (18.5°N, 17.8°E) in western India. The aerosol loading across IND is tremendously complex and tied to the monsoon system, with local and transported dust from the west and mixed urban/industrial and smoke (from a variety of sources) over the IGP and elsewhere [e.g., *Yadav and Rajaman*, 2004; *Ramanathan et al.*, 2005; *Gautam et al.*, 2011; *Henriksson et al.*, 2011]. Aerosol over Pune is from similar sources, with dust from the Thar Desert and Arabian Peninsula most common from May–September and optical dominance of industrial/biomass-burning sources at other times of the year [*Devara et al.*, 2014]. The IGP is also one of the areas of largest disagreement between DB and DT (Figure 4). On comparison with AERONET, the difference in seasonality at sites in the IGP can be traced to DB underestimating AOD and DT overestimating AOD, to different extents at different sites, and these biases being largest in the monsoonal months (July/August) and smallest in DJF. Thus, both algorithms report a similar overall shape of seasonality but DB underesti-

mates and DT overestimates the magnitude of seasonal variability of AOD. These errors are, to an extent, averaged out in the merge, which takes data from both algorithms at different times of year. For most of these sites, the biases typically lie within or close to the algorithms' expected uncertainty, and overall performance is very similar. However, for Pokhara (28.2°N, 84.0°E), Jaipur (26.9°N, 76.8°E), and Karachi (24.9°N, 67.0°E), the latter two being arid areas with a strong dust influence, DB more persistently underestimates AOD. The DB underestimation of AOD at these last two sites are found in all seasons, suggesting perhaps an overestimated surface reflectance and/or overestimated aerosol SSA. Because of the arid surface cover, DB spatial coverage is much higher than DT. Overall, DT performs best in this region (Tables 2, 3), although the merged SDS may provide superior seasonality over both DB and DT, due to opposing seasonal biases in and near the IGP.

5.5. Summary and Looking Forward

The Collection 6 reprocessing of MODIS aerosol products is the result of the cumulative effort of many groups, not only the MODIS science teams but also groups working to maintain the calibration of the sensors, groups involved in ground-based aerosol monitoring, and groups who have used and analysed previous versions of the data sets in detail. Both the DB and DT algorithms have been updated and this study has sought to provide a comparison of the two to help illustrate their regional and global similarities and differences, and to provide some recommendations for data usage. Whichever algorithm is chosen for a particular analysis, it is strongly advised that data users apply the quality assurance (QA) filters provided with the data sets, and the C6 products contain some prefiltered SDSs for this purpose (Table 1).

Comparison against AERONET is the standard method for evaluation of AOD retrieved from spaceborne sensors and represents the best that can be done on a large scale. Algorithm refinements between different data versions, while generally physically based, are still normally evaluated in terms of changes in validation statistics against AERONET; thus, the C6 algorithms (and others) are inherently optimised to a degree against these AERONET sites. As such identified regional/contextual errors are useful to make recommendations about which of DB and/or DT to use, but it is not guaranteed that these can be transferred quantitatively to represent the (unknown) retrieval error away from AERONET sites. Users should bear this important point in mind.

Due to the complexity of the global Earth (surface and atmospheric) system, and the optimization of the algorithms for global rather than regional applications, neither algorithm consistently performs better than the other. To make some general comments, over much of the global land surface, the AOD retrieved by the algorithms and the level of agreement with AERONET are similar, such that it may not matter for many applications which of DB or DT a user chooses. DT often has a better correlation with AERONET than DB, but DB has (outside of tropical regions) greater spatial coverage, and tends to have smaller error compared to AERONET values in low-AOD conditions. DB and DT often exhibit much smaller AOD differences than would be expected given their estimated individual uncertainties, which should not be taken to mean that they have converged on the truth, but is a reminder that they should not be considered to be independent data sets.

Despite the improvements from C5 to C6 various aerosol/surface type-dependent uncertainties have been identified in both algorithms and are often similar to those identified in the C5 land data sets [e.g., *Hyer et al.*, 2011; *Shi et al.*, 2013], notably some systematic (and often opposing) biases in high-AOD conditions and for elevated scenes. Thus, bias correction techniques developed for the C5 over-land data sets [*Hyer et al.*, 2011; *Shi et al.*, 2013] are likely to remain applicable, although specific coefficients will need to be recalculated. The continued presence of some of these contextual biases in C6 suggests that to remove them in future data versions may require a larger-scale overhaul of the underlying physical basis of the retrievals, rather than minor refinements. Conversely, in a few areas (for example, the DT algorithm in India; cf. Figure 1 of *Levy et al.* [2013]), the C6 data can differ significantly from the previous C5. As a result, it is possible that some results obtained using older version(s) of MODIS data may differ quantitatively.

A new feature of C6 is the "merged" SDS, designed with the intention of providing a single data set combining the best of DB and DT into a data product with fewer gaps. MODIS aerosol product users are encouraged to make their own decisions about which data set(s) to use for their particular needs, given the similarities and differences between the two algorithms. This is a nontrivial task, and the C6 merged SDS represents a first attempt in this direction. The analysis has shown that, while not optimal (i.e., not persistently outperforming DB/DT), the current merged SDS nevertheless does provide a data set which will be suitable for

quantitative scientific applications. In particular, as only DB provides coverage over deserts, and there is only one over-ocean algorithm, the merged SDS is useful as a more spatially complete data set than was available previously from these MODIS data products.

This study has provided an overview and initial analysis of the MODIS Aqua C6 products, with the intent of introducing users to key features of the data sets and their differences, and provide a first comparative validation. An individual study is necessarily limited in scope, and further studies will be able to expand upon this to improve the characterization of the new data sets. This analysis has considered only MODIS Aqua data, as Terra data are not available at present. It is expected that results for Terra will be quantitatively similar, although there may be subtle differences, as were found in C5 [e.g., *Levy et al.*, 2010], due to a combination of sensor calibration and sampling a slightly different part of the local diurnal cycle. The release of MODIS Terra data will also enable comparison of the C6 aerosol products with those from the Multiangle Imaging Spectroradiometer (MISR) [*Martonchik et al.*, 1998; *Kahn et al.*, 2010], which also flies on Terra. This analysis focused on AOD at 550 nm, which is the primary data product from both algorithms. Some work has been done to evaluate AOD at other wavelengths and α from DB data [*Sayer et al.*, 2013]; these products have been removed or relegated to "diagnostic" status in the C6 DT data set due to limited information content of the measurements [*Levy et al.*, 2010]. Additional important future work should include analysis of current and historical field campaign data, as well as case studies of extreme events (to identify aerosol-related issues) and some low-AOD cases (to identify regional differences and issues related to surface reflectance treatment), which will assist further in understanding and refinement of both the DB/DT retrieval algorithms and the data "merging" procedure.

Acknowledgments

This work was supported by the NASA EOS program, managed by H. Maring. M.-J. Jeong's work was supported by the Korea Meteorological Administration Research and Development Program under Grant CATER 2012-2064. The authors gratefully acknowledge the AERONET team and site PIs for the creation and stewardship of the Sun-photometer data records, as well as useful comments pertaining to individual sites: I. Abboud, S. F. Abdullaev, J. Agnew, N. X. Anh, A. Ansmann, P. Artaxo, A. Bais, A. C. Banks, F. Baret, C. J. Bruegge (Caltech/JPL), V. E. Cachorro Revilla, M. L. Cancillo Fernandez, A. Chaikovsky, B. Chatenet, H.-B. Chen, N. Chubarova, A. L. Contreras, S. Corradini, E. Cuevas-Agullo, G. Dedieu, P. C. S. Devara, S. Dorado, B. Duchemin, T. F. Eck, V. Fioletov, D. Griffith, B. Gross, P. Goloub, W. M. Hao, B. N. Holben, J. Huang, S. Janjai, A. Karnieli, Y. J. Kim, C. M.B. Lehmann, G. de Leeuw, p. Lestari, N.-H. Lin, P.-H. Lin, K.-N. Liou, J. A. M. Lozano, D. Meyer, R. Mitchell, M. J. Montero-Martinez, F. Morais, J. P. Morel, B. Mougenot (CESBIO, Toulouse, France), N. T. O'Neill, M. Panchenko, A. Panday, S. Payra, E. B. Pereira, M. R. Perrone, A. Pietruczuk, S. Piketh, R. T. Pinker, E. Quel, J. L. Rajot, K. Repasky, J. A. Shaw, A. M. Silva, R. P. Singh, A. Sinyuk, A. Smirnov, P. Sobolewski, G. Stensaas, S. Teggi, D. Tanré, S. N. Tripathi, J. R. Vande Castle, C. Walthall, P. Wang, I. H. Woodhouse, X. Xia, W. Zhang, and G. Zibordi. Site managers, especially those in remote areas, and supporting institutions are also thanked for their extensive efforts. The Bratts Lake and Egbert AERONET sites are also part of AEROCAN, and the support of Environment Canada and the Université de Sherbrooke is acknowledged for these. The Chilbolton site's instrument is provided by the Natural Environment Research Council (NERC) Facilities for Science. The Australian sites are affiliated with AeroSpan, and the support of CSIRO is acknowledged. The MODIS Characterization Support Team and Ocean Biology Processing Group are thanked for their extensive efforts in maintaining the high radiometric quality of MODIS data. L. A. Remer, A. Marshak, and other attendees at NASA GSFC's AeroCenter seminar series are thanked for their comments on an early version of this analysis, as is R. Simmon (NASA GSFC) for useful discussions on graphics and color palettes. AERONET data are available from aeronet.gsfc.nasa.gov and MODIS data from ladsweb.nascom.nasa.gov. F.-M. Bréon and two anonymous reviewers are thanked for helpful comments, which have improved the manuscript.

References

Banks, J. R., H. E. Brindley, C. Flamant, M. J. Garay, N. C. Hsu, O. V. Kalashnikov, L. Klüser, and A. M. Sayer (2013), Intercomparison of satellite dust retrieval products over the west African Sahara during the Fennec campaign in June 2011, *Remote Sens. Environ.*, *136*, 99–116, doi:10.1016/j.rse.2013.05.003.

Bennouna, Y. S., V. E. Cachorro, C. Toledano, A. Berjon, N. Prats, D. Fuertes, R. Gonzalez, R. Rodrigo, B. Torres, and A. M. de Frutos (2011), Comparison of atmospheric aerosol climatologies over southwestern Spain derived from AERONET and MODIS, *Remote Sens. Environ.*, *115*(5), 1272–1284, doi:10.1016/j.rse.2011.01.011.

Bréon, F. M., A. Vermeulen, and J. Descloitres (2011), An evaluation of satellite aerosol products against sunphotometer measurements, *Remote Sens. Environ.*, *115*(12), 3102–3111, doi:10.1016/j.rse.2011.06.017.

Chew, B. N., J. R. Campbell, J. S. Reid, D. M. Giles, E. J. Welton, S. V. Salinas, and S. C. Liew (2011), Tropical cirrus cloud contamination in sun photometer data, *Atmos. Environ.*, *45*(37), 6724–6731, doi:10.1016/j.atmosenv.2011.08.017.

Devara, P. C. S., S. Kumar, K. Vijayakumar, and G. Pandithurai (2014), Sun-sky radiometer synthesis of interplay between aerosols and monsoon activity over Pune, India, *Pure Appl. Geophys.*, *171*, 1–17, doi:10.1007/s00024-014-0828-5.

Dey, S., and L. Di Girolamo (2011), A decade of change in aerosol properties over the Indian subcontinent, *Geophys. Res. Lett.*, *38*, L14811, doi:10.1029/2011GL048153.

Drury, E., D. J. Jacob, J. Wang, R. J. D. Spurr, and K. Chance (2008), Improved algorithm for MODIS satellite retrievals of aerosol optical depths over western North America, *J. Geophys. Res.*, *113*, D16204, doi:10.1029/2007JD009573.

Eck, T. F., B. N. Holben, J. S. Reid, O. Dubovik, A. Smirnov, N. T. O'Neill, I. Slutsker, and S. Kinne (1999), Wavelength dependence of the optical depth of biomass burning, urban, and desert dust aerosols, *J. Geophys. Res.*, *104*(D24), 31,333–31,349.

Eck, T. F., et al. (2013), A seasonal trend of single scattering albedo in southern African biomass-burning particles: Implications for satellite products and estimates of emissions for the world's largest biomass-burning source, *J. Geophys. Res. Atmos.*, *118*, 6414–6432, doi:10.1002/jgrd.50500.

Fast, J. D., et al. (2007), A meteorological overview of the MILAGRO field campaigns, *Atmos. Chem. Phys.*, *7*, 2233–2257, doi:10.5194/acp-7-2233-2007.

Garg, A., P. R. Shukla, and M. Kapshe (2006), The sectoral trends of multigas emissions inventory of India, *Atmos. Environ.*, *40*, 4608–4620, doi:10.1016/j.atmosenv.2006.03.045.

Gautam, R., N. C. Hsu, and K.-M. Lau (2010), Premonsoon aerosol characterization and radiative effects over the Indo-Gangetic Plains: Implications for regional climate warming, *J. Geophys. Res.*, *115*, D17208, doi:10.1029/2010JD013819.

Gautam, R., et al. (2011), Accumulation of aerosols over the Indo-Gangetic Plains and southern slopes of the Himalayas: Distribution, properties and radiative effects during the 2009 pre-monsoon season, *Atmos. Chem. Phys.*, *11*, 12,841–12,863, doi:10.5194/acp-11-12841-2011.

Gautam, R., N. C. Hsu, T. F. Eck, B. N. Holben, S. Janjai, T. Jantarach, S.-C. Tsay, and W. K. Lau (2013), Characterization of aerosols over the Indochina peninsula from satellite-surface observations during biomass burning pre-monsoon season, *Atmos. Environ.*, *78*, 51–59, doi:10.1016/j.atmosenv.2012.05.038.

Guffanti, M., T. J. Casadevall, and K. Budding (2010), Encounters of aircraft with volcanic ash clouds: A compilation of known incidents, 1953-2009, *Tech. rep.*, U. S. Geological Survey, Data Series 545, ver. 1.0. [Available at http://pubs.usgs.gov/ds/545/.]

Hasekamp, O. P., and J. Landgraf (2007), Retrieval of aerosol properties over land surfaces: Capabilities of multi-viewing-angle intensity and polarization measurements, *Appl. Opt.*, *46*(16), 3332–3344, doi:10.1364/AO.46.003332.

Henriksson, S. V., A. Laaksonen, V.-M. Kerminen, P. Räisänen, H. Järvinen, A.-M. Sundström, and G. de Leeuw (2011), Spatial distributions and seasonal cycles of aerosols in India and China seen in global climate-aerosol model, *Atmos. Chem. Phys.*, *11*, 7975–7990, doi:10.5194/acp-11-7975-2011.

Holben, B. N., et al. (1998), AERONET: A federated instrument network and data archive for aerosol characterization, *Remote Sens. Environ.*, *66*, 1–16, doi:10.1016/S0034-4257(98)00031-5.

Hsu, N. C., S.-C. Tsay, M. D. King, and J. R. Herman (2004), Aerosol properties over bright-reflecting source regions, *IEEE Trans. Geosci. Remote Sens.*, *42*(3), 557–569, doi:10.1109/TGRS.2004.824067.

Hsu, N. C., R. Gautam, A. M. Sayer, C. Bettenhausen, C. Li, M. J. Jeong, S.-C. Tsay, and B. N. Holben (2012), Global and regional trends of aerosol optical depth over land and ocean using SeaWiFS measurements from 1997 to 2010, *Atmos. Chem. Phys.*, *12*, 8037–8053, doi:10.5194/acp-12-8037-2012.

Hsu, N. C., M.-J. Jeong, C. Bettenhausen, A. M. Sayer, R. Hansell, C. S. Seftor, J. Huang, and S.-C. Tsay (2013), Enhanced Deep Blue aerosol retrieval algorithm: The second generation, *J. Geophys. Res. Atmos.*, *118*, 9296–9315, doi:10.1002/jgrd.50712.

Huang, J., N. C. Hsu, S.-C. Tsay, Z. Liu, M. J. Jeong, R. A. Hansell, and J. Lee (2013), Use of spaceborne lidar for the evaluation of thin cirrus contamination and screening in the Aqua MODIS Collection 5 aerosol products, *J. Geophys. Res. Atmos.*, *118*, 6444–6453, doi:10.1002/jgrd.50504.

Huete, A., K. Didan, W. van Leeuwen, T. Miura, and E. Glenn (2011), MODIS vegetation indices, *Land Remote Sens. Global Environ. Change*, *11*, 579–602, doi:10.1007/978-1-4419-6749-7_26.

Hyer, E. H., J. S. Reid, and J. Zhang (2011), An over-land aerosol optical depth data set for data assimilation by filtering, correction, and aggregation of MODIS Collection 5 optical depth retrievals, *Atmos. Meas. Tech.*, *4*, 379–408, doi:10.5194/amt-4-379-2011.

Ichoku, C., D. A. Chu, S. Mattoo, Y. J. Kaufman, L. A. Remer, D. Tanré, I. Slutsker, and B. N. Holben (2002), A spatio-temporal approach for global validation and analysis of MODIS aerosol products, *Geophys. Res. Lett.*, *29*(12), MOD1-1–MOD1-4, doi:10.1029/2001GL013206.

Jethva, H., S. K. Satheesh, J. Srinivasan, and R. C. Levy (2010), Improved retrieval of aerosol size-resolved properties from moderate resolution imaging spectroradiometer over India: Role of aerosol model and surface reflectance, *J. Geophys. Res.*, *115*, D18213, doi:10.1029/2009JD013218.

Kahn, R. A. (2012), Reducing the uncertainties in direct aerosol radiative forcing, *Surv. Geophys.*, *33*(3–4), 701–721, doi:10.1007/s10712-011-9153-z.

Kahn, R. A., B. J. Gaitley, M. J. Garay, D. J. Diner, T. F. Eck, A. Smirnov, and B. N. Holben (2010), Multiangle Imaging SpectroRadiometer global aerosol product assessment by comparison with the Aerosol Robotic Network, *J. Geophys. Res.*, *115*, D23209, doi:10.1029/2010JD014601.

Kahn, R. A., M. J. Garay, D. L. Nelson, R. C. Levy, M. A. Bull, D. J. Diner, J. V. Martonchik, E. G. Hansen, L. A. Remer, and D. Tanré (2011), Response to "Toward unified satellite climatology of aerosol properties: 3. MODIS versus MISR versus AERONET", *J. Quant. Spectrosc. Radiat. Transfer*, *112*(5), 901–909, doi:10.1016/j.jqsrt.2010.11.001.

Karnieli, A., Y. J. Kaufman, L. A. Remer, and A. Wald (2001), AFRI—Aerosol free vegetation index, *Remote Sens. Environ.*, *71*(1), 10–21, doi:10.1016/S0034-4257(01)00190-0.

Kaufman, Y. J., A. E. Wald, L. A. Remer, B.-C. Gao, R.-R. Li, and L. Flynn (1997), The MODIS 2.1μm channel-correlation with visible reflectance for use in remote sensing of aerosol, *IEEE Trans. Geosci. Remote Sens.*, *35*(5), 1286–1298, doi:10.1109/36.628795.

Kinne, S., et al. (2006), An AeroCom initial assessment—Optical properties in aerosol component modules of global models, *Atmos. Chem. Phys.*, *6*, 1815–1834, doi:10.5194/acp-6-1815-2006.

Kokhanovsky, A. A., and G. de Leeuw (Eds.) (2009), *Aerosol Remote Sensing Over Land*, Springer, Berlin.

Kokhanovsky, A. A., et al. (2010), The inter-comparison of major satellite aerosol retrieval algorithms using simulated intensity and polarization characteristics of reflected light, *Atmos. Meas. Tech.*, *3*, 909–932, doi:10.5194/amt-3-909-2010.

Levy, R. C., L. A. Remer, S. Mattoo, E. F. Vermote, and Y. J. Kaufman (2007), Second-generation operational algorithm: Retrieval of aerosol properties over land from inversion of Moderate Resolution Imaging Spectroradiometer spectral reflectance, *J. Geophys. Res.*, *112*, D13211, doi:10.1029/2006JD007811.

Levy, R. C., L. A. Remer, R. G. Kleidman, S. Mattoo, C. Ichoku, R. Kahn, and T. F. Eck (2010), Global evaluation of the Collection 5 MODIS dark-target aerosol products over land, *Atmos. Chem. Phys.*, *10*, 103,999–10,420, doi:10.5194/acp-10-10399-2010.

Levy, R. C., S. Mattoo, L. A. Munchak, L. A. Remer, A. M. Sayer, F. Patadia, and N. C. Hsu (2013), The Collection 6 MODIS aerosol products over land and ocean, *Atmos. Meas. Tech.*, *6*, 2989–3034, doi:10.5194/amt-6-2989-2013.

Li, G. B., H. S. Yuan, N. Feng, and S. Tao (2009), Comparing MODIS and AERONET aerosol optical depth over China, *Int. J. Remote Sens.*, *30*(24), 6519–6529, doi:10.1080/01431160903111069.

Li, Z., F. Niu, K.-H. Lee, J. Xin, W.-M. Hao, B. Nordgren, Y. Wang, and P. Wang (2007), Validation and understanding of moderate resolution imaging spectroradiometer aerosol products (C5) using ground-based measurements from the handheld Sun photometer network in China, *J. Geophys. Res.*, *112*, D22S07, doi:10.1029/2007JD008479.

Li, Z., X. Zhao, R. Kahn, M. Mishchenko, L. Remer, K.-H. Lee, M. Wang, I. Laszlo, T. Nakajima, and H. Maring (2009), Uncertainties in satellite remote sensing of aerosols and impact on monitoring its long-term trend: A review and perspective, *Ann. Geophys.*, *27*, 2755–2770, doi:10.5194/angeo-27-2755-2009.

Martonchik, J. V., D. J. Diner, R. A. Kahn, T. P. Ackerman, M. M. Verstraete, B. Pinty, and H. R. Gordon (1998), Techniques for the retrieval of aerosol properties over land and ocean using multiangle imaging, *IEEE Trans. Geosci. Remote Sens.*, *36*, 4, doi:10.1109/36.701027.

Meister, G., and B. A. Franz (2011), Adjustments to the MODIS Terra radiometric calibration and polarization sensitivity in the 2010 reprocessing, paper presented at SPIE 8153, Earth Observing Systems 16, 815308, doi:10.1117/12.891787, 13 Sept.

Meister, G., B. A. Franz, E. J. Kwiatkowska, and C. R. McClain (2012), Corrections to the calibration of MODIS Aqua ocean color bands derived from SeaWiFS data, *IEEE Trans. Geosci. Remote Sens.*, *50*(1), 310–319, doi:10.1109/TGRS.2011.2160552.

Mishchenko, M. I., I. V. Geogdzhayev, B. Cairns, B. E. Carlson, J. Chowdhar, A. A. Lacis, L. Liu, W. B. Rossow, and L. . D. Travis (2007), Past, present, and future of global aerosol climatologies derived from satellite observations: A perspective, *J. Quant. Spectrosc. Radiat. Transfer*, *106*, 325–347, doi:10.1016/j.jqsrt.2007.01.007.

Mishchenko, M. I., L. Liu, L. D. Travis, B. Cairns, and A. A. Lacis (2010), Toward unified satellite climatology of aerosol properties: 3. MODIS versus MISR versus AERONET, *J. Quant. Spectrosc. Radiat. Transfer*, *111*(4), 540–552, doi:10.1016/j.jqsrt.2009.11.003.

Murphy, D. M. (2009), Effect of stratospheric aerosols on direct sunlight and implications for concentrating solar power, *Environ. Sci. Technol.*, *43*(8), 2784–2786, doi:10.1021/es802206b.

O'Neill, N. T., A. Ignatov, B. N. Holben, and T. F. Eck (2000), The lognormal distribution as a reference for reporting aerosol optical depth statistics; Empirical tests using multi-year, multi-site AERONET Sunphotometer data, *Geophys. Res. Lett.*, *27*(20), 3333–3336, doi:10.1029/2000GL011581.

Pandithurai, G., R. T. Pinker, O. Dubovik, B. N. Holben, and T. Aro (2001), Remote sensing of aerosol optical characteristics in sub-Sahel, West Africa, *J. Geophys. Res.*, *106*(D22), 28,347–28,356, doi:10.1029/2001JD900234.

Petrenko, M., C. Ichoku, and G. Leptoukh (2012), Multi-sensor Aerosol Products Sampling System (MAPSS), *Atmos. Meas. Tech.*, *5*, 913–926, doi:10.5194/amt-5-913-2012.

Piketh, S. J., H. J. Annegarn, and P. D. Tyson (1999), Lower tropospheric aerosol loadings over South Africa: The relative contribution of aeolian dust, industrial emissions, and biomass burning, *J. Geophys. Res.*, *104*(D1), 1597–1607, doi:10.1029/1998JD100014.

Pope, C. A., III, R. T. Burnett, M. J. Thun, E. E. Calle, D. Krewski, K. Ito, and G. D. Thurston (2002), Lung cancer, cardiopulmonary mortality, and long-term exposure to fine particulate air pollution, *J. Am. Med. Assoc.*, *287*(9), 1132–1141, doi:10.1001/jama.287.9.1132.

Qin, Y., and R. M. Mitchell (2009), Characterisation of episodic aerosol types over the Australian continent, *Atmos. Chem. Phys.*, *9*, 1943–1956, doi:10.5194/acp-9-1943-2009.

Ramanathan, V., C. Chung, D. Kim, T. Bettge, L. Buja, J. T. Kiehl, W. M. Washington, Q. Fu, D. R. Sikka, and M. Wild (2005), Atmospheric brown clouds: Impacts on South Asian climate and hydrological cycle, *Proc. Natl. Acad. Sci. U.S.A.*, *102*(15), 5326–5333, doi:10.1073/pnas.0500656102.

Ramanathan, V., M. V. Ramana, G. Roberts, D. Kim, C. E. Corrigan, C. E. Chung, and D. Winker (2007), Warming trends in Asia amplified by brown cloud solar absorption, *Nature*, *448*, 575–578, doi:10.1038/nature06019.

Reid, J. S., et al. (2013), Observing and understanding the Southeast Asian aerosols system by remote sensing: An initial review and analysis for the Seven Southeast Asian Studies (7 SEAS) program, *Atmos. Res.*, *122*, 303–468, doi:10.1016/j.atmosres.2012.06.005.

Remer, L. A., S. Mattoo, R. C. Levy, and L. A. Munchak (2013), MODIS 3 km aerosol product: Algorithm and global perspective, *Atmos. Meas. Tech.*, *6*, 1829–1844, doi:10.5194/amt-6-1829-2013.

Roberts, G., M. J. Wooster, and E. Lagoudakis (2009), Annual and diurnal African biomass burning temporal dynamics, *Biogeosciences*, *6*, 849–866, doi:10.5194/bg-6-849-2009.

Salinas, S. V., B. N. Chew, N. Mohamad, and S. C. Liew (2013), First measurements of aerosol optical depth and Angstrom exponent number from AERONET's Kuching site, *Atmos. Env.*, *78*, 231–241, doi:10.1016/j.atmosenv.2013.02.016.

Sayer, A. M., A. Smirnov, N. C. Hsu, L. A. Munchak, and B. N. Holben (2012a), Estimating marine aerosol particle volume and number from Maritime Aerosol Network data, *Atmos. Chem. Phys.*, *12*, 8889–8909, doi:10.5194/acp-12-8889-2012.

Sayer, A. M., N. C. Hsu, C. Bettenhausen, M.-J. Jeong, B. N. Holben, and J. Zhang (2012b), Global and regional evaluation of over-land spectral aerosol optical depth retrievals from SeaWiFS, *Atmos. Meas. Tech.*, *5*, 1761–1778, doi:10.5194/amt-5-1761-2012.

Sayer, A. M., N. C. Hsu, C. Bettenhausen, and M.-J. Jeong (2013), Validation and uncertainty estimates for MODIS Collection 6 "Deep Blue" aerosol data, *J. Geophys. Res. Atmos.*, *118*, 7864–7872, doi:10.1002/jgrd.50600.

Schonbrödt, F. D., and M. Perugini (2013), At what sample size do correlations stabilize?, *J. Res. Pers.*, *47*(5), 609–612, doi:10.1016/j.jrp.2013.05.009.

Schulz, M., et al. (2006), Radiative forcing by aerosols as derived from the AeroCom present-day and pre-industrial simulations, *Atmos. Chem. Phys.*, *6*, 5225–5246, doi:10.5194/acp-6-5225-2006.

Shi, Y., J. Zhang, J. S. Reid, B. N. Holben, E. J. Hyer, and C. Curtis (2011), An analysis of the Collection 5 MODIS over-ocean aerosol optical depth product for its implication in aerosol assimilation, *Atmos. Chem. Phys.*, *11*, 557–565, doi:10.5194/acp-11-557-2011.

Shi, Y., J. Zhang, J. S. Reid, E. J. Hyer, and N. C. Hsu (2013), Critical evaluation of the MODIS Deep Blue aerosol optical depth product for data assimilation over North Africa, *Atmos. Meas. Tech.*, *6*, 949–969, doi:10.5194/amt-6-949-2013.

Smirnov, A., B. N. Holben, T. F. Eck, O. Dubovik, and I. Slutsker (2000), Cloud-screening and quality control algorithms for the AERONET database, *Remote Sens. Environ.*, *73*(3), 337–349.

Tanré, D., Y. J. Kaufman, M. Herman, and S. Mattoo (1997), Remote sensing of aerosol properties over oceans using the MODIS/EOS spectral radiances, *J. Geophys. Res.*, *102*(D14), 16,971–16,988, doi:10.1029/96JD03437.

Tian, R. X., and J. An (2013), Relationship between aerosol transport routes and red tide occurrences in the East China Sea, *Environ. Earth Sci.*, *69*(5), 1499–1508, doi:10.1007/s12665-012-1984-5.

van der Werf, G. R., J. T. Randerson, L. Giglio, G. J. Collatz, M. Mu, P. S. Kasibhatla, D. C. Morton, R. S. DeFries, Y. Jin, and T. T. van Leeuwen (2010), Global fire emissions and the contribution of deforestation, savanna, forest, agricultural, and peat fires (1997–2009), *Atmos. Chem. Phys.*, *10*, 11,707–11,735, doi:10.5194/acp-10-11707-2010.

van Donkelaar, A., R. Martin, M. Braur, R. Kahn, R. Levy, C. Verduzco, and P. Villeneuve (2010), Global estimates of exposure to fine particulate matter concentrations from satellite-based aerosol optical depth, *Environ. Health Perspect.*, *118*, 847–855, doi:10.1289/ehp.0901623.

Wang, L. L., Y. S. Wang, J. Y. Xin, Z. Q. Li, and X. Wang (2010), Assessment and comparison of three years of Terra and Aqua MODIS aerosol optical depth retrieval (C005) in Chinese terrestrial regions, *Atmos. Res.*, *97*(1–2), 229–240, doi:10.1016/j.atmosres.2010.04.004.

Wu, A. S., X. X. Xiong, D. R. Doelling, D. Morstad, A. Angal, and R. Bhatt (2013), Characterization of Terra and Aqua MODIS VIS, NIR, and SWIR spectral bands' calibration stability, *IEEE Trans. Geosci. Remote Sens.*, *51*(7), 4330–4338, doi:10.1109/TGRS.2012.2226588.

Yadav, S., and V. Rajaman (2004), Geochemistry of aerosols of northwestern part of India adjoining the Thar desert, *Geochim. Cosmochim. Acta*, *68*(9), 1975–1988, doi:10.1016/j.gca.2003.10.032.

Zelazowski, P., A. M. Sayer, G. E. Thomas, and R. G. Grainger (2011), Reconciling satellite-derived atmospheric properties with fine-resolution land imagery: Insights for atmospheric correction, *J. Geophys. Res.*, *116*, D18308, doi:10.1029/2010JD015488.

Zhang, J., and J. S. Reid (2006), MODIS aerosol product analysis for data assimilation: Assessment of over-ocean level 2 aerosol optical thickness retrievals, *J. Geophys. Res.*, *111*, D22207, doi:10.1029/2005JD006898.